H4.SMR.582 - 5

SCHOOL ON MATERIALS FOR ELECTRONICS: GROWTH, PROPERTIES AND APPLICATIONS

18 NOVEMBER - 6 DECEMBER 1991

"LIQUID PHASE EPITAXY"

E. KUPHAL
Deutsche Bundespost Telekom
FI - Forschungsinstitut
Referat/Section: FI 41a
P.O. Box 10 00 03
D-6100 Darmstadt
Germany

These are preliminary lecture notes, intended only for distribution to participants

Liquid Phase Epitaxy

E. Kuphal

Deutsche Bundespost Telekom, Forschungsinstitut, P.O. Box 100003, W-6100 Darmstadt,
Fed. Rep. Germany

Abstract. This paper presents a comprehensive review of the method of liquid phase epitaxy (LPE) of semiconductors. In Sect. 1 the physical principles including diffusion-limited growth and solid-liquid phase diagrams are treated in detail. In Sect. 2 technological aspects and various kind of growth systems including industrial versions are described. Section 3 summarizes the relevant properties of LPE grown layers. Section 4 contains the application of LPE to the material system InP/InGaAs/InGaAsP as a model system. In Sect. 5 the advantages and weaknesses of LPE with respect to device applications in comparison with competing methods are discussed, and finally we attempt to predict the future direction of LPE.

Since its invention by Nelson in 1963 [1] liquid phase epitaxy (LPE) has proved to be a versatile, flexible method to grow thin layers of III–V, II–VI and IV–VI compounds for material investigations and device applications. Many "firsts" of electronic and optoelectronic devices were based on LPE structures. One important example was the GaAs/GaAlAs double-heterostructure (DH) laser diode continuous-wave (cw) lasing at room temperature [2, 3]. Also, the cw operation of DH lasers emitting at wavelengths beyond 1 μm, realized in the systems InP/InGaAsP [4], GaAsSb/GaAlAsSb [5] and GaSb/GaAlAsSb [6], was first successfully achieved with LPE material.

Examples of photodetectors for longer wavelengths made for the first time by LPE are the pin-photodiodes in the systems InP/InGaAsP [7], InP/InGaAs [8] and GaSb/GaAlSb [9] and the avalanche photodiodes in the systems InP/InGaAsP [10], InP/InGaAs [11], GaSb/GaSb/GaAlSb [9] and the avalanche photodioded in the systems InP/InGaAsP [10], InP/InGaAs [11], GaSb/GaAlSb [12] and GaSb/GaAlAsSb [13]. The first monolithically integrated planar Gunn devices [14], integrated bipolar transistor-laser circuits [15] and InGaAs pin-FET photoreceivers [16] were also based on LPE material. The same holds for recent developments such as the first InGaAsP three-terminal phototransistors [17], the InGaAsP distributed Bragg reflector lasers [18], the InGaAsP distributed feedback lasers [19, 20], the InGaAsP multi-quantum-well lasers [21] and the rare earth doped

InGaAsP injection lasers [22]. These are only a few examples, and this list could easily be continued. The exploration and development of many devices and materials was only possible due to the existing LPE technique so that many years were saved prior to the advent of other epitaxial techniques.

LPE yields a high crystalline quality in terms of structural perfection owing to the fact that it is near-equilibrium process. The supersaturations required for growth are very low and are of the order of a few Kelvin. LPE allows high purity layers to be produced, particularly in cases where the solvent species are constituents of the semiconductor compound or alloy. Moreover, it is possible to grow very thin layers in the range of a few nm by means of LPE. On the other hand, growth rates are sufficiently high to permit the growth of layers with thicknesses up to 100 μm.

The technological equipment required for LPE is relatively inexpensive. Compared to vapour phase epitaxy the LPE technique is inherently safer, because the raw materials and the waste products are less toxic and not pyrophoric. Therefore, one requires neither a big air conditioning system nor a gas supply system (except for H_2) whose installation is very expensive and time-consuming in the case of VPE or MOVPE. Moreover, the deposition efficiency of grown epitaxial material is relatively high in LPE, in contrast to all other epitaxial techniques. The growth solutions can be resaturated for many applications and recycled. The waste products of the LPE

process consist only of the solidified metallic solutions, which are unproblematic.

These and other benefits make LPE the standard method for several device applications in research and production. Many companies that are now gradually moving into MOVPE or MBE still rely on LPE as their stand-by technique.

Some excellent reviews on the LPE technique have already been written by Dawson (1972) [23], by Panish and Ilegems on phase equilibria (1972) [24], by Kressel and Nelson (1973) [25], a special issue of the Journal of Crystal Growth on LPE (1974) [26], by Giess and Ghez (1975) [26a], by Casey and Panish (1978) [27], by Benz and Bauser (1980) [28], by Hsieh (1980) [29], by Stringfellow (1982) [30] and by Nakajima (1985) [31].

In the past few years there have been many new developments in LPE which make this technique attractive for the future as well. These include automation of the growth process for better layer thickness control, melt casting systems fo facilitate the work of weighing the source materials, larger wafer areas up to 50 mm in diameter, multiple-wafer boats, refined boat constructions, better control of the layer morphology and a deeper theoretical understanding. It is the aim of this work to provide an overview and describe the more recent developments of the LPE technique and to critically compare it with competing epitaxial methods.

1. Physical Principles of the LPE Process

1.1 General Considerations

Liquid phase epitaxy means the growth of thin films from metallic solutions on a crystalline, oriented substrate. The solvent element can either be a constituent of the growing solid, e.g. In or Ga, or it can be some other low-melting metal like Sn, Bi or Pb, which is incorporated into the solid only as a dopant. The solvent contains a small quantity of a solute, e.g. As in Ga, which is transported towards the liquid–solid interface. The process is controlled best if this transport occurs only be diffusion, i.e. the driving force in the solution is a concentration gradient of the solute, as shown in Fig. 1. The growth boats are commonly designed such that, essentially, only diffusion perpendicular to the interface occurs; convection and surface-tension-related transport are suppressed. The latter two types of transport are suppressed if the following requirements are fulfilled: Temperature gradients in the solution should be as small as possible, and both the height, h, and the radius of curvature (caused by surface tension) of the solution should be small compared to the lateral dimension of the substrate. With these constraints the LPE process can be treated as a one-dimensional diffusion process, and the growth rate is diffusion-limited. The larger the substrate area, the smaller is the influence of edge effects and the better is the homogeneity of the layer properties.

The thermodynamic driving force for LPE is generated by cooling the system below the liquidus (or saturation) temperature T_s of the liquid-solid phase diagram, which
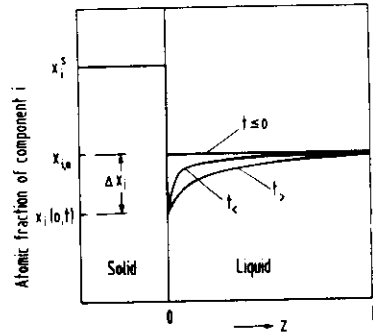

Fig. 1. Schematic representation of the atomic fractions of component i in the liquid and solid brought into contact at $t = 0$. The z-axis denotes the growth direction
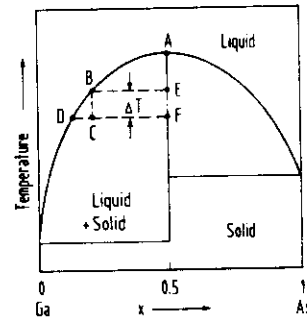

Fig. 2. Schematic phase diagram of a binary III–V system (Ga–As). x denotes the mole fraction of As
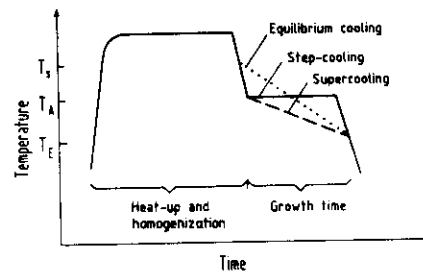

Fig. 3. Typical temperature–time profile during epitaxy

is shown schematically for GaAs in Fig. 2. While melt growth is performed at the melting point A (1238° C), solution growth such as LPE takes place at much lower temperatures (600–800° C), which provides a better crystalline quality than melt growth does. Point B on the liquidus represents a Ga-rich liquid saturated with As. On cooling the system by the supersaturation ΔT, it moves to point C, which is in the two-phase region, so that a driving force exists for the precipitation of GaAs until point D on the liquidus line is reached, where precipitation comes to an end. The original supersaturation is then removed. During growth, the solid moves from point E to point F. Since the solid composition is stoichiometric for all binary compounds, the composition is the same at both points. This is no longer true in the case of ternary or quaternary alloys, where the solid composition depends on the supersaturation. If the system is heated

above T_s, material is dissolved from the substrate until the solution is saturated. Thus, LPE allows deposition and etch-back within the same growth run.

An LPE technique consists in providing mechanisms for: (a) supersaturation of the solution, (b) introduction of the substrate upon which growth will occur, (c) removing the substrate from the solution after the growth time t. The typical temperature-time profile applied to the system is given in Fig. 3: The system is heated up to a temperature above T_s in order to obtain a homogeneous mixture of the solution constituents. Then it is cooled down, and the substrate is brought into contact with the solution at the starting temperature T_A. Growth is determined at the end temperature T_E by removal of the substrate, and the furnace is subsequently cooled down quickly to avoid thermal degradation of the grown layer. Three different types of cooling techniques are commonly used, which cause different growth rates and layer morphologies:

a) Steep-cooling or isothermal growth. Growth is started at a supersaturation $\Delta T = T_s - T_A$, and the temperature remains constant at $T = T_A = T_E$ during growth. This method is particularly interesting, because if the solution volume is sufficiently large, ΔT remains constant and the system can be represented by a fixed point in the phase diagram. This situation is the only one where the growth law can be derived even for an arbitrary multicomponent system.

b) Equilibrium-cooling. T_A is equal to T_s, and the system is linearly cooled to T_E at the cooling rate α.

c) Supercooling. The starting temperature is $T_A < T_s$, and the system is linearly cooled to T_E. This technique corresponds to a superposition of step-cooling and equilibrium-cooling.

1.2 Solution of the Diffusion Equation

The macroscopic growth rate v perpendicular to the phase boundary can be evaluated by a treatment of the phase diagrams (thermodynamics) and using diffusion theory. The solution of the diffusion equation depends on the boundary conditions determined by the above-mentioned cooling techniques. In this section a consistent theoretical description of the growth rate will be given for the following cases: (a) the general multi-component system, (b) the binary system, and (c) the ternary system. In Sect. 1.3 the phase diagrams will be treated. A comparison with experimental results will be given in Sect. 4.

The liquid solution is usually described by the atomic fractions x_i of its constituents, where

$$\sum x_i = 1, \tag{1}$$

whereas in practice the weights W_i of the solution components are known. The relations between these quantities are quoted here because they are needed later. The quaternary In–Ga–As–P solution including an elemental dopant is chosen as an example. The solution consists of GaAs + InAs + InP + dopant diluted in In. We define

$$W_1 = W_{GaAs}/W_{In}, \qquad W_2 = W_{InP}/W_{In},$$
$$W_3 = W_{InAs}/W_{In}, \qquad W_4 = W_{dop}/W_{In} \tag{2}$$

$$F_1 = A_{In}/(A_{Ga} + A_{As}), \qquad F_2 = A_{In}/(A_{In} + A_P),$$
$$F_3 = A_{In}/(A_{In} + A_{As}), \qquad F_4 = A_{In}/A_{dop}, \tag{3}$$

where the W_i are weights relative to the weight of the solvent, and the F_i are ratios of the respective atomic weights; W_4 and F_4 correspond to the dopant. The atomic fractions are then:

$$x_{As} = (F_1 W_1 + F_3 W_3)/N_w, \qquad x_p = F_2 W_2/N_w$$
$$x_{Ga} = F_3 W_3/N_w, \qquad x_{dop} = F_4 W_4/N_w \tag{4}$$

with

$$N_w = 1 + 2F_1 W_1 + 2F_2 W_2 + 2F_3 W_3 + F_4 W_4. \tag{5}$$

x_{In} follows from (1). If, however, the atomic fractions are given, the corresponding relative weights are found to be

$$W_1 = x_{Ga}/(N_x F_1), \qquad W_2 = x_p/(N_x F_2)$$
$$W_3 = (x_{As} - x_{Ga})/(N_x F_3), \qquad W_4 = x_{dop}/(N_x F_4) \tag{6}$$

with

$$N_x = 1 - 2x_{As} - 2x_p - x_{dop}. \tag{7}$$

Substitution of (6) into (5) yields

$$N_w = 1/N_x. \tag{8}$$

1.2.1 Growth Rate for an $n + 1$-Component System

In this section the general case of an $n + 1$-component system is treated. We consider only the diffusional mass transport in a supersaturated liquid, which is sufficient to describe most of the growth situations. Undersaturated solutions and the diffusion in the solid which can be relevant in certain heterostructure growth situations as investigated by Small and Ghez [32] are neglected here. Also kinetic effects (e.g. dependence on crystallographic orientation) are neglected. The diffusion in the liquid is treated here as a one-dimensional problem; see Fig. 1. There are $n + 1$ mass fluxes, one for each component. Since the sum of all mole fractions is unity, only n fluxes have to be considered. According to Fick's second law we obtain n diffusion equations [33]:

$$\frac{\partial x_i}{\partial t} = \frac{\partial}{\partial z}\left(\sum_{j=1}^{n} D_{ij} \frac{\partial x_j}{\partial z}\right) + \frac{v(t)}{F} \frac{\partial x_i}{\partial z}. \tag{9}$$

Here D_{ij} is the diffusion matrix. The term containing the growth rate $v(t)$ comes in due to the motion of the phase boundary $v(t)/F$. The factor F is the ratio of the atomic density in the liqudid (at the growth temperature T_G) to that in the solid (at room temperature)

$$F = \frac{\varrho_l M_s}{m \varrho_s M_l}, \tag{10}$$

where ϱ_l and M_l are the density and the averaged molecular weight of the liquid, ϱ_s and M_s are the density and molecular weight of the solid, and m is the number of atoms per formular unit of the solid (2 for III-V

compounds). For a zincblende structure, F can also be expressed as

$$F = \frac{a_0^3 \varrho_1 N_A}{8 M_1} \qquad (11)$$

with the lattice constant a_0 and Avogadro's constant N_A. Some values of F are 1.15 for GaAs, 0.97 for InP and 0.96 for $In_{0.53}Ga_{0.47}As$.

If we consider only isothermal growth (step-cooling), the time dependence of the growth rate can be determined.

At $t = 0$ the solution is assumed to be homogeneously mixed:

$$x_i(z, 0) = x_{i,0}. \qquad (12)$$

As shown in Fig. 1, the boundary conditions at the free surface of the semi-infinite solution $(h = \infty)$ are

$$x_i(\infty, t) = x_{i,0}. \qquad (13)$$

The mole fractions at the phase boundary $(z = 0)$ are

$$x_i(0, t) = x_{i,0} - \Delta x_i(t), \qquad (14)$$

where $\Delta x_i(t)$ is the supersaturation of the component i at the phase boundary. In addition, there are n flux conditions, caused by the law of mass conservation:

$$v(t) [x_i^s - x_i(0, t)] = \sum_{j=1}^{n} D_{ij} \frac{\partial x_j}{\partial z} \Bigg|_{z=0} F. \qquad (15)$$

Here, x_i^s is the mole fraction of component i in the solid. In the binary case, there is no influence of the flux condition on the solution of the diffusion equation. In the general case, however, the flux conditions cause a connection of the gradients at the phase boundary, since obviously there is only one common growth rate. Thus, the diffusion equations of the different components are still connected:

$$\left(\sum_{k=1}^{n} D_{ik} \frac{\partial x_k}{\partial z} \Bigg|_{z=0} \right) \Bigg/ \left(\sum_{k=1}^{n} D_{jk} \frac{\partial x_k}{\partial z} \Bigg|_{z=0} \right)$$

$$= \frac{x_i^s - x_i(0, t)}{x_j^s - x_j(0, t)}. \qquad (16)$$

In the case of isothermal deposition, the time dependence of the growth rate $v(t)$ can be obtained from the general system of diffusion equations. By the Boltzmann transformation

$$\xi = z/\sqrt{t} \qquad (17)$$

the partial differential equations (9) can be reduced to ordinary differential equations

$$-\frac{\xi}{2t} \frac{\partial x_i}{\partial \xi} = \frac{1}{\sqrt{t}} \frac{\partial}{\partial \xi} \left(\sum_{j=1}^{n} D_{ij} \frac{1}{\sqrt{t}} \frac{\partial x_i}{\partial \xi} \right)$$

$$+ \frac{v(t)}{F} \frac{1}{\sqrt{t}} \frac{\partial x_i}{\partial \xi}. \qquad (18)$$

The same transformation has to be applied to the boundary conditions (12–14) and the flux condition (15). It can be seen immediately that the time t can be eliminated
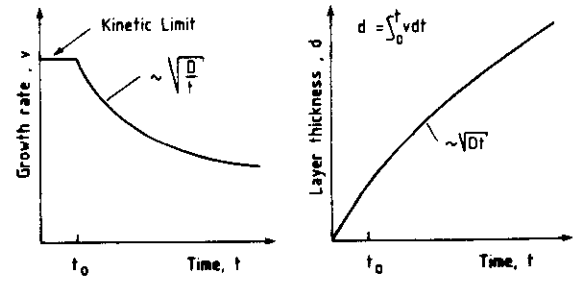

Fig. 4. Growth rate and layer thickness for growth limited by kinetics and diffusion

from (18) and from the transformed flux conditions only if

$$v(t) \propto 1/\sqrt{t} \qquad (19)$$

and if $\Delta x_i(t)$ in (14) is constant $(\Delta x_i(t) = \Delta x_i)$. Thus, it is shown that even in a system containing $n + 1$ components (i.e. with n^2 diffusion coefficients) the epitaxial layer thickness follows the $\sqrt{t}$-law [33]. Figure 4 shows this general result. The figure also depicts that for very short growth times $t < t_0$ the growth rate is no longer diffusion-limited but controlled by the kinetics of the incorporation of the atoms into the lattice (depending on surface steps, dislocations etc.). Our experiments on InP show that the $\sqrt{t}$-law is valid at least down to $t = 300$ ms.

Furthermore, a second important conclusion can be drawn: If $x_i(0, t)$ in (14) and (16) is independent of time, the solid compositions x_i^s are also constant as long as an equilibrium exists at the phase boundary. And $x_i(0, t)$ is time-independent if the supersaturation Δx_i remains constant. The supersaturation is time-independent if the solution is semi-infinitely extended and T_G is constant. This means that under isothermal growth conditions the LPE of mixed crystals with an arbitrary number of components is free of compositional grading. This result is obtained simply by a discussion of the boundary conditions, without solving the diffusion equation explicitly and without making any assumptions on the diffusion matrix D_{ij}. Of course, it is not valid for the case of linear cooling of the solution. There, a linear dependence of the x_i^s on t is found in a first approximation, which means a compositional grading in mixed crystals.

For dilute solutions, as used in LPE, non-diagonal elements of the diffusion matrix D_{ij} seem to be negligible, since the interaction between the dilute components is very small. In the following it is therefore assumed that the non-diagonal elements are zero. This allows us to calculate the layer thickness explicitly [33]. In this case (9) is simplified to n decoupled equations with n diffusion coefficients D_i. If we further neglect the motion of the phase boundary, the solution for the mole fractions is:

$$x_i(z, t) = x_{i,0} - \Delta x_i \operatorname{erfc} \left(\frac{z}{2\sqrt{D_i t}} \right). \qquad (20a)$$

The error-function complement is defined as

$$\operatorname{erfc}(x) = 1 - \frac{2}{\sqrt{\pi}} \int_0^x \exp(-\lambda^2) \, d\lambda. \qquad (20b)$$

From (20) the gradients at the phase boundary can be calculated. Insertion into (16) yields a connection of the supersaturations at the phase boundary:

$$\frac{\Delta x_i \sqrt{D_i}}{\Delta x_j \sqrt{D_j}} = \frac{x_i^s - x_i(0,t)}{x_j^s - x_j(0,t)}. \tag{21}$$

a) Step-cooling ($\Delta T \neq 0, \alpha = 0$). The growth rate can be calculated from one of the equations (15), say for component 1. $\partial x_i / \partial z$ follows from (20) as

$$\left.\frac{\partial x_i}{\partial z}\right|_{z=0} = \frac{\Delta x_i}{\sqrt{\pi D_i t}}. \tag{22}$$

The supersaturations Δx_i of the n components can be replaced by the supersaturation expressed in temperature ΔT. This can be obtained from an approximation of the isothermal liquidus surface in the $n+1$-dimensional space by its tangential plane

$$\Delta T = \sum_{i=1}^{n} \frac{\partial T}{\partial x_i} \Delta x_i. \tag{23}$$

Together with (21), (23) becomes

$$\Delta T = \frac{\Delta x_1 \sqrt{D_1}}{x_1^s - x_1} \sum_{i=1}^{n} \frac{\partial T}{\partial x_i} \frac{x_i^s - x_i}{\sqrt{D_i}}. \tag{24}$$

Solving (24) for Δx_1 and inserting it into (22), and then substituting $\partial x_1 / \partial z$ into (15), we obtain for the growth rate

$$v = \frac{K \Delta T}{2\sqrt{t}}, \tag{25}$$

where

$$K(T) = \frac{2F}{\sqrt{\pi}} \left(\sum_{i=1}^{n} \frac{\partial T}{\partial x_i} \frac{x_i^s - x_i}{\sqrt{D_i}} \right)^{-1}. \tag{26}$$

Integration of (25) over t gives the layer thickness for isothermal growth

$$d_A = K \Delta T \sqrt{t}. \tag{27}$$

b) Equilibrium-cooling ($\Delta T = 0, \alpha \neq 0$). In this case the atomic fractions at the phase boundary can be approximated by linear functions of time with α being the cooling rate:

$$x_i(0,t) = x_{i,0} - \alpha t \frac{\partial x_i}{\partial T}. \tag{28}$$

After a similar calculation [34] we get

$$d_\alpha = \frac{2}{3} K \alpha t^{3/2} \tag{29}$$

with the same constant K as in (26).

c) Supercooling ($\Delta T \neq 0, \alpha \neq 0$). Supercooling is the most frequently used cooling technique. As it is the superposition of step-cooling and equilibrium-cooling, the layer thicknesses may be added in a first approximation:

$$d = d_A + d_\alpha = K \left(\Delta T \sqrt{t} + \frac{2}{3} \alpha t^{3/2} \right). \tag{30}$$

The constant $K(T)$ contains the phase diagram quantities, which will be treated in Sect. 1.3. If these quantities

are unknown, the layer thickness of any $n+1$-component system can, nevertheless, be calculated easily, if K is determined empirically from one single growth experiment. The step-cooling contribution in (30) dominates for short growth times, and the equilibrium-cooling part can be neglected as long as

$$t \ll \frac{3\Delta T}{2\alpha}. \tag{31}$$

If the temperature changes as in cooling techniques (b) and (c), a compositional grading of the growing layer occurs. The temperature dependence of the atomic fractions in the solid x_i^s can be described by a linear approximation, where the surfaces of the x_i^s in the $n+1$-dimensional space are replaced by their tangential planes similar to (23):

$$\Delta x_j^s = \sum_{i=1}^{n} \frac{\partial x_j^s}{\partial x_i} \Delta x_i. \tag{32}$$

Substitution of Δx_1 from (24) into (32) yields as an important result the dependence of the solid composition of the growth temperature (or supersaturation):

$$\frac{\Delta x_j^s}{\Delta T} = \left(\sum_{i=1}^{n} \frac{\partial x_j^s}{\partial x_i} \frac{x_i^s - x_i}{\sqrt{D_i}} \right) \Big/ \left(\sum_{i=1}^{n} \frac{\partial T}{\partial x_i} \frac{x_i^s - x_i}{\sqrt{D_i}} \right). \tag{33}$$

1.2.2 Growth Rate for a Binary System

In binary systems we only have to deal with one atomic fraction x and one diffusion coefficient D of the solute, and the solid composition is $x^s = 1/2$.

The maximum layer thickness d_{max}. To get an estimate of the layer thickness, it is useful to calculate its upper limit d_{max}, which is deposited within a given cooling span after a very long growth time. This means that all dissolved material between point B and D in Fig. 2 is precipitated. d_{max} depends only on the solution height h and the phase diagram, if we assume that the solution area is equal to the substrate area. It does not depend on the diffusion coefficient or the cooling technique applied. This situation is realized by means of the "thin solution" technique, where all material is grown out after a sufficiently long time. d_{max} follows from the condition that the number of atoms in the solid is equal to the number of atoms precipitated from the liquid:

$$d_{max} = c_1 \left(\frac{x(T_s)}{N_x(T_s)} - \frac{x(T_E)}{N_x(T_E)} \right), \tag{34}$$

$$c_1 = \varrho_l M_s \frac{h}{\varrho_s A_l}. \tag{35}$$

where ϱ_s and M_s are the density and the molecular weight of the solid, and ϱ_l and A_l the density and the atomic weight of the solvent, respectively. N_x is defined in (7). For the example of GaAs grown from a doped Ga solution, $N_x = 1\text{-}2x_{As} - x_{dop}$. For mixed alloys d_{max} cannot be calculated in a simple way because the composition of the growing layer changes upon cooling, and the "crystallization path" in the phase diagram depends on the diffusion coefficients of the different solutes.

Liquid Phase Epitaxy

Layer thickness for a semi-infinite solution. On the assumption of a semi-infinite solution – see boundary condition (13) – the layer thickness for step-cooling and equilibrium-cooling is identical with (30). The constant K from (26) reads, for a binary system:

$$K = \frac{2F}{(1/2) - x(0,t)} \sqrt{\frac{D}{\pi}} \frac{\partial x}{\partial T}, \tag{37}$$

where $\partial x/\partial T$ is the slope of the liquidus from Fig. 2. In many cases the atomic fraction of the solute is $x \ll 1$, and $F \ll 1$, so that K is approximately

$$K \approx 4 \sqrt{\frac{D}{\pi}} \frac{\partial x}{\partial T}. \tag{38}$$

Equations (30) and (38) which have been derived from the general $(n+1)$-component case are in full agreement with the derivation by Hsieh [35] based on the binary system.

Layer thickness for a finite solution. In contrast to the general $n+1$-component system, for the binary system it is also possible to calculate the layer thickness for the practical case of growth from a finite solution of height h. This has been done by Moon [36] for the sep-cooling

$$d_A = d_{A,\max} \left(1 - 2 \sum_{n=0}^{\infty} \frac{\exp(-\lambda_n^2 Dt/h^2)}{\lambda_n^2}\right) \tag{39}$$

and for the equilibrium-cooling mode

$$d_\alpha = d_{\alpha,\max} \left[1 + \frac{2}{Dt/h^2} \left(\sum_{n=0}^{\infty} \frac{\exp(-\lambda_n^2 Dt/h^2)}{\lambda_n^4} - \frac{1}{6}\right)\right], \tag{40}$$

where $\lambda_n = (n+1/2)\pi$. The maximum layer thicknesses for the two cooling techniques are found in analogy to (34) to be

$$d_{A,\max} = c_1 \left(\frac{x(T_s)}{N_x(T_s)} - \frac{x(T_A)}{N_x(T_A)}\right), \tag{41}$$

$$d_{\alpha,\max} = c_1 \left(\frac{x(T_A)}{N_x(T_A)} - \frac{x(T_E)}{N_x(T_E)}\right), \tag{42}$$

$$d_{\max} = d_{A,\max} + d_{\alpha,\max}. \tag{43}$$

The terms in brackets in (39) and (40) can be interpreted as the deposition efficiencies of the two cooling techniques.

By computer calculation we have verified that (39) and (40) for the finite solution numerically agree with (27) and (29) for the semi-infinite solution in the limit $Dt/h^2 \ll 1$. For increasing values of Dt/h^2, (27) and (29) tend to overestimate the true thicknesses, but the error in both cases remains less than 10% as long as $Dt/h^2 < 0.7$. Therefore, it can be stated as a rule of thumb that the simple equations (27) and (29) are applicable as long as the "diffusion length" $\sqrt{Dt}$ is smaller than the solution height.

1.2.3 Growth Rate for a Ternary System

The formulae given for the $n + 1$-component system are easier to understand in the simpler case of a ternary sys-
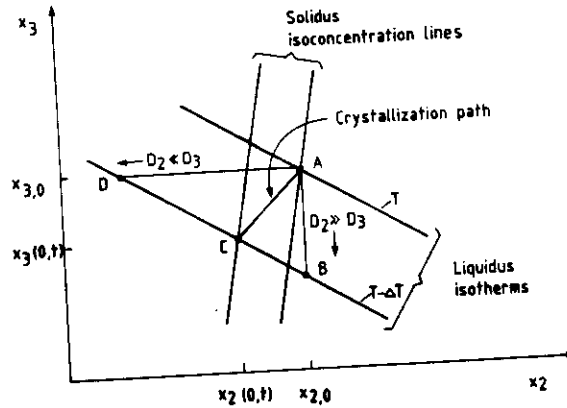

Fig. 5. Schematic phase diagram of a ternary system

tem. The phase diagram of this system in shown schematically in Fig. 5. Here x_1 denotes the atomic fraction of the solvent, and x_2, x_3 and D_2, D_3 are the atomic fractions and diffusion coefficients of the dissolved components, respectively. The growth temperature no longer defines a point on the liquidus curve, as in the binary system, but an isothermal line on the liquidus surface. When we grow a layer from a given liquidus composition (point A) supersaturated by ΔT, the composition of partial thermodynamic equilibrium (point C) is unknown at first. If the distribution coefficients of the solutes are larger than one, as is the case e.g. for InGaAs grown from an In solution or GaAlAs from a Ga solution, we can state the following: Point C lies on the isotherm between points B and D, and depends on the ratio D_2/D_3. The limiting points B and D hold for the cases $D_2 \gg D_3$ and $D_2 \ll D_3$, respectively.

The coordinates of point C defining the crystallization path follow from (24):

$$x_2(0,t) = x_{2,0} - \Delta T \frac{x_2^s - x_2}{\sqrt{D_2}}$$

$$\times \left(\frac{\partial T}{\partial x_2} \frac{x_2^s - x_2}{\sqrt{D_2}} + \frac{\partial T}{\partial x_3} \frac{x_3^s - x_3}{\sqrt{D_3}}\right)^{-1}, \tag{44}$$

$$x_3(0,t) = x_{3,0} - \Delta T \frac{x_3^s - x_3}{\sqrt{D_3}}$$

$$\times \left(\frac{\partial T}{\partial x_2} \frac{x_2^s - x_2}{\sqrt{D_2}} + \frac{\partial T}{\partial x_3} \frac{x_3^s - x_3}{\sqrt{D_3}}\right)^{-1}, \tag{45}$$

For isothermal growth from a sufficiently large solution, points A and C are time independent, i.e. the solid composition is constant during growth, but it depends linearly on ΔT. For the example of $In_{1-x}Ga_xAs$ the indices 1, 2 and 3 refer to In, Ga and As, respectively, and

$$x_2^s = x/2, \quad x_3^s = 1/2. \tag{46}$$

The solid composition at point C follows from (33) as

$$x_2^s(C) = x_2^s(A) - \Delta T$$

$$\times \frac{\frac{\partial x_2^s}{\partial x_2} \frac{x_2^s - x_2}{\sqrt{D_2}} + \frac{\partial x_2^s}{\partial x_3} \frac{x_3^s - x_3}{\sqrt{D_3}}}{\frac{\partial T}{\partial x_2} \frac{x_2^s - x_2}{\sqrt{D_2}} + \frac{\partial T}{\partial x_3} \frac{x_3^s - x_3}{\sqrt{D_3}}}. \tag{47}$$

- 6 -

The layer thickness for both isothermal growth d_Δ and equilibrium cooling d_α is again identical with (30), where the constant K is derived from (26) to be

$$K(T) = \frac{2F}{\sqrt{\pi}} \left(\frac{\partial T}{\partial x_2} \frac{x_2^s - x_2}{\sqrt{D_2}} + \frac{\partial T}{\partial x_3} \frac{x_3^s - x_3}{\sqrt{D_3}} \right)^{-1}. \qquad (48)$$

Equations (30) and (48) are identical to the result in [Ref. 33, eq. 13] given in another notation, and are very similar to the form given in [37].

A comparison of the layer thicknesses in the binary system (37) and ternary system (48) shows that the thickness of, for instance, InGaAs is less than that of InAs grown under the same conditions from In-rich solutions. This is due to the facts that $\partial x_{As}/\partial T$ decreases with increasing concentration of Ga and a second positive term occurs in the denominator of (48). We have verified this result experimentally. Correspondingly, it has been found in the GaAlAs system that $d(\text{GaAlAs}) < d(\text{GaAs})$ under identical growth conditions [38,39].

1.3 Phase Diagrams of III–V Systems

To evaluate the formulae given in Sect. 1.2 for the layer thickness, the growing solid and its compositional grading, the following quantities must be known: the diffusion coefficient $D_i(T)$, the saturation temperature as a function of the liquidus composition $T_s(x_i)$, the solid composition x_i^s in equilibrium with the given liquid solution, and the partial derivatives $\partial T/\partial x_i$ and $\partial x_i^s/\partial x_j$.

The diffusion coefficient is, in general, taken as a free parameter and determined by measurements of the layer thickness. The remaining quantities are derived from a phase diagram model, which contains only a few adjustable parameters. For III–V compounds the regular solution model [24] has proved to be very successful.

1.3.1 Phase Diagram of the Binary System

A detailed derivation of the phase diagram based on the regular solution model was given by Casey and Panish [27] and by Stringfellow [30]. The result for the binary system is:

$$RT \ln[4x(1-x)]$$
$$+\Delta S_F(T_F - T) + 2(1/2 - x)^2 \alpha(T) = 0. \qquad (49)$$

Here, ΔS_F and T_F are the entropy and temperature of fusion of the III–V compound, respectively, $R = 1.9872\,\text{cal}/(\text{mole K})$ the gas constant and $\alpha(T)$ the liquid interaction parameter. Equation (49) describes the liquidus curve $x(T)$, which is schematically shown in Fig. 2. Under the condition of very dilute solutions ($x \ll 1$), which is fulfilled at low temperatures and, usually, under LPE conditions, (49) becomes

$$x = \frac{1}{4} \exp(\Delta S_F/R) \exp[-(\Delta S_F T_F + \alpha/2)/RT]. \qquad (50)$$

Thus, the liquidus curve has got the simple form of an exponential function of $1/T$, an approximation which

has often been adopted in the literature [29,40]. Experimentally it has been found that for many binary systems $\alpha(T)$ has a linear temperature dependence:

$$\alpha(T) = a + bT, \qquad (51)$$

where a and b are constants. Equation (50) can then be written as

$$x = \frac{1}{4} \exp[(\Delta S_F - b)/R] \exp[-(\Delta S_F T_F + a)/RT]. \qquad (52)$$

a and b are determined by adjusting (49) or (52) to the measured liquidus curve. Frequently the entropy of fusion is not well known. An uncertainty in ΔS_F causes a modification in a and b while maintaining the same functional relationship for $x(T)$ in (52). Therefore, sets of values of T_F, ΔS_F and $\alpha(T)$ are tabulated [24,27] together with the understanding that a modification of one implies a modification of the other. The interaction parameters for III–V liquid solutions generally vary between 0 and $-6000\,\text{cal/mole}$, which is indicative of a fairly weak attractive interaction. The negative α of, for instance, the Ga-rich Ga–As solution suggests that Ga–As quasi-compounds are formed in the liquid. The vanishing α of, for example, the Ga–Sn solution means that no interaction between the species of the solution exists ("ideal solution").

The slope $\partial x/\partial T$ of the liquidus curve needed for the LPE layer thickness in (37) or (38) is now easily derived from (52). Experimental diffusion coefficients of the solute in the metallic liquid are in the range $D = (0.3–30) \times 10^{-5}\,\text{cm}^2/\text{s}$. The resulting constant K of (37) varies between 0.003 and 0.1 $\mu\text{m}/(\text{K}\sqrt{\text{s}})$ depending on the material and the growth temperature, which is chosen between reasonable limits. If we admit values of ΔT between 1 K and 10 K, the layer thickness after $t = 1\,\text{s}$ according to (30) is in the range

$$d = 1.5–500\,\text{nm}. \qquad (53)$$

The lower limit is about one order of magnitude higher than the lower limit of the (time-independent) growth rate of the MOVPE or MBE technique, whereas the higher limit exceeds the growth rate of the other techniques by far.

1.3.2 Phase Diagram of the Ternary System Including Strain

In the past the phase equilibria of ternary III–V crystalline solid solutions were studied mainly because of the importance of GaAlAs for DH lasers. The ternary $\text{III}_{1-x}\text{–III}'_x\text{–V}$ is considered to be a pseudobinary alloy composed of $(1-x)$ moles of the binary III–V and x moles of III'–V. The corresponding applies to III–V–V' compounds. Consequently, the theory contains a further parameter, namely the solid interaction parameter α_{1323} between the two binaries. In addition, three liquid interaction parameters α_{ij} as well as one entropy and one temperature of fusion for each of the two binaries are needed. The functions of the regular solution model are derived in [24, 25, 27, 30]. Panish [41] even gives the

model functions for a system containing three components in the solid and four components in the liquid, i.e. including a doping element, whose solubility in the solid is neglected. The latter formulae can also be applied to the case where the solvent element is not a constituent of the alloy, e.g. GaAlAs grown from a Sn-rich solution. The solid interaction parameter α_{1323} of the ternary is commonly adjusted to the experimental data. It can, however, also be deduced from the delta-lattice-parameter (DLP) model [42]. In this model the α_{1323} is shown to depend only on the relative lattice mismatch $\Delta a/a$ between the two constituting binaries.

The regular solution model successfully describes the phase diagram of GaAlAs obtained experimentally [27, 43]. In the heterosystem of GaAlAs grown on GaAs substrate almost no strain occurs, because the lattice constants of GaAs and AlAs are almost equal $(\Delta a/a = 1.3 \times 10^{-3})$. In ternary heterosystems like $In_{1-x}Ga_xP/GaAs$ or $In_{1-x}Ga_xAs/InP$, however, large mismatches of up to 3.8% are possible. For these systems the above-mentioned model still predicts the liquid composition sufficiently well, but fails for the solid composition. The model can also be successfully applied to these mismatched systems provided the strain is taken into account, as will be shown in the following.

The contribution of the substrate-induced strain to the liquid–solid equilibrium is taken into account in the regular solution model by adding the elastic strain energy in the layer to the Gibbs free enthalpy of the solid. It is assumed that the lattice mismatch is so small that only elastic deformation of the lattice occurs, but no relaxation of the stress due to creation of misfit dislocations. Furthermore, the layer thickness is assumed to be very thin compared to the substrate thickness so that substrate bending caused by the mismatch can be neglected. The molar elastic strain energy can then be written [33]

$$W = \psi_{hkl}\left(\frac{a-a_0}{a_0}\right)^2, \tag{54}$$

where a and a_0 are the lattice constant of the layer and the substrate, respectively. The orientation-dependent factor ψ_{hkl} becomes, for (100)-oriented substrates,

$$\psi_{100} = V_m(c_{11} + c_{12} - 2c_{12}^2/c_{11}). \tag{55}$$

For the (110)-orientation we find

$$\psi_{110} = V_m\left[4c_{44} + c_{11} - 2\frac{(c_{12} - 2c_{44})^2}{2c_{44} + c_{11} + c_{12}}\right] \tag{56}$$

and for the (111)-orientation

$$\psi_{111} = V_m\frac{6c_{44}(c_{11} + 2c_{12})}{4c_{44} + c_{11} + 2c_{12}}. \tag{57}$$

V_m denotes the mole volume. c_{11}, c_{12} and c_{44} are the three elastic constants of cubic crystals, which are tabulated for III–V compounds in [44].

By differentiation of (54) with respect to the number of moles of the two binary subsystems we obtain the chemical potential associated with the strain energy. Insertion of these terms into the regular solution model

then gives [33]:

$$RT \ln\left(\frac{4x_1x_3}{x_{13}}\right) - \alpha_{1323}x_{23}^2 - \alpha_{13}/2 + \Delta S_{13}^F(T_{13}^F - T)$$
$$+ RT \ln\gamma_1 + RT \ln\gamma_3 - \frac{\psi_{hkl}}{a_0^2}(a_{13} - a_{23})x_{13}(1 + x_{23})$$
$$- \frac{\psi_{hkl}}{a_0^2}(a_0^2 - a_{23}^2 + 2a_{13}a_{23} - 2a_0a_{13}) = 0; \tag{58}$$

$$RT \ln\left(\frac{4x_2x_3}{x_{23}}\right) - \alpha_{1323}x_{13}^2 - \alpha_{23}/2 + \Delta S_{23}^F(T_{23}^F - T)$$
$$+ RT \ln\gamma_2 + RT \ln\gamma_3 + \frac{\psi_{hkl}}{a_0^2}(a_{13} - a_{23})^2x_{13}^2$$
$$- \frac{\psi_{hkl}}{a_0^2}(a_0 - a_{23})^2 = 0. \tag{59}$$

Here, the x_i are the mole fractions in the liquid and the x_{ij} those in the solid solution. The α_{ij} and α_{1323} are the interaction parameters in the liquid and in the solid, ΔS_{ij}^F and T_{ij}^F are the entropy and temperature of fusion, respectively. The a_{ij} are the lattice constants. For the calculations the elastic constants and the lattice constants have to be taken at the growth temperature. The activity coefficients γ_1, γ_2, and γ_3 in the liquid are given by Panish [41]:

$$RT \ln\gamma_1$$
$$= \alpha_{12}x_2^2 + \alpha_{13}x_3^2 + \alpha_{14}x_4^2 + x_2x_3(\alpha_{12} + \alpha_{13} - \alpha_{23})$$
$$+ x_2x_4(\alpha_{12} + \alpha_{14} - \alpha_{24}) + x_3x_4(\alpha_{13} + \alpha_{14} - \alpha_{34}), \tag{60}$$

$$RT \ln\gamma_2$$
$$= \alpha_{12}x_1^2 + \alpha_{23}x_3^2 + \alpha_{24}x_4^2 + x_1x_3(\alpha_{12} + \alpha_{23} - \alpha_{13})$$
$$+ x_3x_4(\alpha_{23} + \alpha_{24} - \alpha_{34}) + x_1x_4(\alpha_{12} + \alpha_{24} - \alpha_{14}), \tag{61}$$

$$RT \ln\gamma_3$$
$$= \alpha_{13}x_1^2 + \alpha_{23}x_2^2 + \alpha_{34}x_4^2 + x_1x_2(\alpha_{13} + \alpha_{23} - \alpha_{12})$$
$$+ x_2x_4(\alpha_{23} + \alpha_{34} - \alpha_{24}) + x_1x_4(\alpha_{13} + \alpha_{34} - \alpha_{14}). \tag{62}$$

The ternary phase diagram is given here for the first time including both the strain energy and an arbitrary dopant. The dopant x_4 comes in via (60–62). For the example of $In_{1-x}Ga_xAs$ the indices 1, 2 and 3 refere to In, Ga and As with

$$x \equiv x_{23} = x_2^s/x_3^s; \tag{63}$$

see (46), and

$$x_{13} + x_{23} = 1. \tag{64}$$

For $Ga_{1-x}Al_xAs$ the indices 1, 2 and 3 refer to Al, Ga and As with $x = x_{13}$.

It should be noted that the inclusion of the strain energy does not lead to an additional free parameter because ψ_{hkl} is determined from the known elastic properties of the crystals. We have solved the system of equations (58–64) numerically by a computer program for three different situations which are of practical interest: (1) x_1 to x_4 are given, x and T are determined; (2) x_1, x_4 and T are given, x, x_2 and x_3 are determined; (3) x, T and x_4 are given, x_1, x_2 and x_3 are determined.

Of course, for $\psi_{hkl} = 0$ the system is reduced to the ordinary ternary phase diagram [24] without strain which is valid for GaAlAs/GaAs. Also the transition to the binary phase diagram is easily carried out: If we set $x_{13} = 1$ and $x_2 = x_4 = 0$ in (58) or $x_{23} = 1$ and $x_1 = x_4 = 0$ in (59), both yield the equation (49) for the binary.

Furthermore, it can be shown that in ternary phase diagrams, too, the solubilities of very dilute solutions. i.e. at low temperatures, can be approximated by exponential function of $1/T$. If we stick to the example of $In_{1-x}Ga_xAs$, the very dilute solution means $x_1 \approx 1$, $x_2 \ll 1$, $x_3 \ll 1$, $x_4 \ll 1$. Equation (58) is then solved for x_3:

$$x_3 = \frac{x_{13}}{4} \exp\left(\frac{\Delta S_{13}^F}{R}\right)$$
$$\times \exp\left(-\frac{\Delta S_{13}^F T_{13}^F + \alpha_{13}/2 + \text{const}}{RT}\right). \qquad (65)$$

An equivalent function is found for x_2 by transformation of the indices. If the solid composition x_{13} is held constant, (65) indeed gives the simple exponential dependence of $1/T$ for the ternary system, which has already been found in (50) for the very dilute binary system.

Kuphal [45] has shown that the solubility data of the In–Ga–As liquid below $T = 660°$ C in equilibrium with lattice-matched $In_{0.53}Ga_{0.47}As/InP$ are very well fitted by a straight line in a $\log x_{Ga}$ vs. $1/T$ and $\log x_{As}$ vs. $1/T$ plot in agreement with (65). This behaviour greatly facilitates the determination of ternary solubility data.

1.3.3 Phase Diagram of a Quaternary System (InGaAsP)

The calculation of III–III'–V–V' type quaternary phase diagrams is rather complex because the mixing of elements on both sublattices must be considered for the thermodynamic treatment of the solid. Models to predict this type of phase diagram have been developed by Stringfellow [42], Ilegems and Panish [46] and Jordan and Ilegems [47]. The most important application of a quaternary system is the alloy $In_{1-x}Ga_xAs_yP_{1-y}$ lattice-matched to InP because of its use in optoelectronic devices, particularly lasers in the wavelength range $\lambda = 1.0–1.65$ μm. Nakajima [31] found only poor agreement between the experimental phase diagram data of InGaAsP and the model of Jordan and Ilegems [47] when he used the liquid and solid interaction parameters, which are valid for binary and ternary systems [24]. De Cremoux [48] obtained a rather good correspondence of the models of Stringfellow [42] and Jordan and Ilegems [47] with InGaAsP liquid-solid data, at least at one temperature (640° C), but was forced to use interaction parameters which deviate from those valid for binary and ternary systems [24, 27]. Perea and Fonstad [49] achieved a good agreement between their data on (111)B substrates and a modified model, but at the expense of ten additional free parameters. None of the models is able to predict the difference in distribution coefficients experimentally found by Hsieh [50] between the (100) and (111)B substrate orientations.

To avoid the above-mentioned difficulties and the need to solve complex model functions, Kuphal [45] has established a purely empirical phase diagram. In this model suitable functions are adjusted to all available measured liquid-solid data in the interesting temperature range between 570 and 660° C. However, the model is only valid for compositions x, y lattice-matched to (100)-oriented InP. As the mole fractions x_{Ga}, x_{As} and x_P are not more than a few percent of the In-solution, the solution is considered to be very dilute. Thus, it is rational to assume the same temperature dependence as was derived for very dilute ternary solutions (cf. (65)), namely $x_i \propto \exp(-1/T)$. The empirical phase diagram reads [45]

$$x_{As} = f_1(x_{Ga}) \exp(-7181/T), \qquad (66)$$

$$x_{Ga} = f_2(x) \exp(-3584/T), \qquad (67)$$

$$x_P = f_3(1 - y) \exp(-11411/T), \qquad (68)$$

where T is the liquidus temperature measured in Kelvin, and the f_i are polynomials given by

$$f_1 = 3.8451 \times 10^4 \, x_{Ga} - 5.6805 \times 10^6 \, x_{Ga}^2$$
$$+ 5.0985 \times 10^8 \, x_{Ga}^3 - 2.6191 \times 10^{10} \, x_{Ga}^4$$
$$+ 7.0231 \times 10^{11} \, x_{Ga}^5 - 7.6075 \times 10^{12} \, x_{Ga}^6, \qquad (69)$$

$$f_2 = 0.70694x + 3.4624x^2 - 8.7492x^3$$
$$+ 36.554x^4 - 32.878x^5, \qquad (70)$$

$$f_3 = 10^2[13.305(1 - y) - 4.7256(1 - y)^2$$
$$+ 12.417(1 - y)^3 - 3.3953(1 - y)^4]. \qquad (71)$$

The functions were found by fitting about 330 published equilibrium data and they hold for a supersaturation $\Delta T \approx 5$ K. The exponential factor of x_{Ga} in (67) is the same as for the ternary compound $In_{0.53}Ga_{0.47}As$ [45], and the exponential factor of x_P in (68) is the same as for InP [45, 51]. Thus, this phase diagram is valid over the full range of compositions and it also correctly reproduces the phase diagrams of the binary and ternary limit of the InGaAsP system.

Besides (66–68) other cuts through the four-dimensional quaternary phase diagram can also be performed. For this purpose we need the relation between x and y for lattice-matched compositions. The lattice mismatch as a function of x and y is found by applying Vegard's law to the lattice constants of the four binary constituents [52]

$$\frac{\Delta a}{a} \equiv \frac{a(x, y) - a(\text{InP})}{a(\text{InP})}$$
$$= 0.03227y - 0.07128x + 0.002214xy. \qquad (72)$$

The condition of lattice matching ($\Delta a/a = 0$) yields

$$x = 0.4527y/(1 - 0.0311y) \qquad (73)$$

$$y = x/(0.4527 + 0.0311x). \qquad (74)$$

For instance $x_{Ga} = x_{Ga}(y, T)$ is found by substitution of (73) into (67); $x_{As} = x_{As}(y, T)$ follows from substitution of $x_{Ga}(y, T)$ into (66), or $x_{As} = x_{As}(x, T)$ from substitution of (74) into $x_{As}(y, T)$. Equations (66–71) have been

successfully used as starting values for LPE growth in several laboratories.

It should be noted, however, that no partial derivatives may be derived from these equations: For example $\partial x_{As}/\partial T$ cannot be obtained by a differentiation of (66), (as was tried by Pan et al. [53]), because all three equations (66–68) are connected, and they are understood to be only jointly applicable to equilibria between lattice-matched solids and corresponding liquid compositions. Experimentally, the following problem often arises: Using a set of starting values x_{As}, x_{Ga} and x_P, e.g. from (66–68), experimental results for λ, $\Delta a/a$, T_s and $T_s - T_G$ are obtained. (The solid with composition parameters x, y is also fully characterized by its gap wavelength λ and its lattice mismatch $\Delta a/a$, the relationship between the two being given in [45]). If these results are to be corrected by $\Delta\lambda$, $\Delta(\Delta a/a)$, ΔT_s and $\Delta(T_s - T_G)$, the necessary corrections to the starting values can be computed from the following system of linear equations:

$$\frac{\partial\lambda}{\partial Z_1}\Delta Z_1 + \frac{\partial\lambda}{\partial Z_2}\Delta Z_2 + \frac{\partial\lambda}{\partial Z_3}\Delta Z_3 + \frac{\partial\lambda}{\partial Z_4}\Delta Z_4 = \Delta\lambda \quad (75)$$

$$\frac{\partial a/a}{\partial Z_1}\Delta Z_1 + \frac{\partial a/a}{\partial Z_2}\Delta Z_2 + \frac{\partial a/a}{\partial Z_3}\Delta Z_3 + \frac{\partial a/a}{\partial Z_4}\Delta Z_4$$
$$= \Delta(\Delta a/a) \quad (76)$$

$$\frac{\partial T_s}{\partial Z_1}\Delta Z_1 + \frac{\partial T_s}{\partial Z_2}\Delta Z_2 + \frac{\partial T_s}{\partial Z_3}\Delta Z_3 + 0 = \Delta T_s \quad (77)$$

with

$$\Delta Z_1 = \Delta x_{As}/x_{As}, \quad \Delta Z_2 = \Delta x_{Ga}/x_{Ga},$$
$$\Delta Z_3 = \Delta x_P/x_P, \quad \Delta Z_4 = \Delta(T_s - T_G). \quad (78)$$

The 11 partial derivatives $\partial\lambda/\partial Z_i$, $(\partial a/a)/\partial Z_i$ and $\partial T_s/\partial Z_i$ have been determined experimentally for the most important compositions x, y [54]. Using this correction routine it was possible to adjust the required gap wavelength to < 10 nm, the lattice mismatch to $< 1\times10^{-4}$ and the saturation temperature to $< 1\,K$. The empirical phase diagram supplemented in this way by its first derivatives is now, of course, also valid for non-lattice-matched compositions, and quantities like the layer thickness (26) or the dependence of the solid composition on supersaturation (33) can be derived.

2. Methodology

The experimental apparatus for growing LPE layers essentially consists of a graphite crucible for the solution and the substrate, contained in a quartz tube, which is flushed by Pd-purified H_2 gas and heated by a temperature-controlled furnace [29]. Four principal techniques – tipping, dipping, sliding and moving by centrifugal force – have been used to initiate and terminate contact between solution and substrate. In addition, a number of other variations, especially for multislice or multilayer growth or growth of ultrathin layers, have been reported.

2.1 Tipping and Dipping Techniques

In the original tipping device of Nelson [1] the whole furnace and quartz tube had to be tipped. In an improved version of Grobe and Salow [55] and Bauser et al. [56] the quartz tube including the crucible is tipped around the longitudinal axis (Fig. 6a). This technique produces excellent layer purity ($\mu = 180000\,cm^2/Vs$ at $T = 77k$ for GaAs [55]). This is due to the fact that the boat design is very simple and the graphite walls are rather thin. It has been shown [57] that the layer purity is the better the thinner the graphite parts are and the less hidden surfaces the boat contains. Secondly, no sliding of graphite parts occurs so that no dust particles can be created by abrasion. The drawbacks are: The thickness homogeneity is only moderate because of two-dimensional diffusion in the solution, only single layers can be grown, and the solution cannot be protected against evaporation of volatile elements.

A combination between a tipping and a slider boat, which allows multilayer growth, has been developed by Kaufmann and Heime [58] (Fig. 6b). The boat consists of several chambers of the type of Bauser's boat, one for each solution, and the solution is brought onto the substrate again by tipping. The substrate is transported by a slider from one compartment into the next when the solution is not in contact with the substrate. An advantage over the conventional sliding technique (Sect. 2.2) is that solution carry-over and scratching of the substrate surface due to sliding is excluded in this version. However, graphite particle abrasion is still possible. Driving this boat is rather complex since it requires rotational as well as translatory motion.

The constructions considered so far have to be rotated forward and backward to start and stop the deposition. As a consequence, thin layers are tapered, because the solution rests for a longer time on one side of the substrate than on the other. This disadvantage is overcome by an improved version of the tipping-slider boat [59], which can be rotated by 360° as shown in Fig. 6c. Several substrates, each $8\,cm^2$ in area, are clamped onto each slider. Source substrates can be introduced, too, in order to saturate the different solutions. The solutions and substrates are loaded when the sliders are in the withdrawn position. To prevent decomposition of the substrates, the length of the sliders (70 cm each) allows the storage of the samples in the cold zone of the system.

The original dipping technique uses a vertical furnace and growth tube with the crucible containing the solution at the lower end. Growth is initiated by lowering the substrate from above to immerse it in the solution. In the version of Holmes and Kamath [60] the crucible contains up to one kg of solution, and one substrate after another can be introduced into the hot zone through an entry vacuum chamber. The dipping technique has been improved for multiwafer growth by two German manufacturers. In these cases a horizontal furnace and up to two large-volume horizontal solution containers are used. One hundred parallel-positioned 2 inch wafers are simultaneously dipped into one solution. The solutions are only used once, but can be recycled. This technique
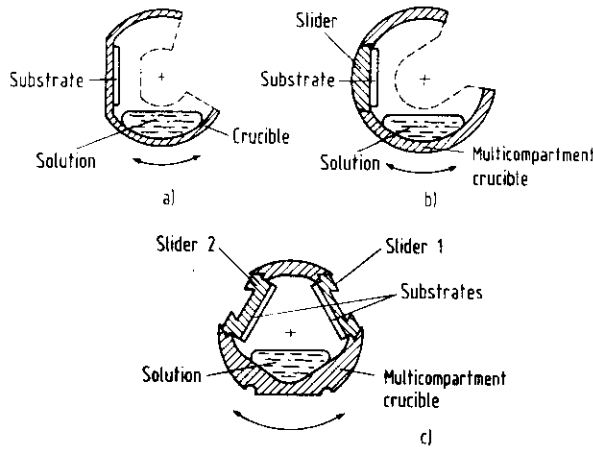
Fig. 6. Different designs of tipping boats: (a) The tipping device after Bauser et al. [56], (b) and (c) tipping-slider boats after Kaufmann et al. [58, 59]

allows double layers to be grown, and it is extremely well suited for the mass production of LED and IRED wafers, where thickness homogeneity is not so important. For this application all other epitaxial techniques are ruled out by costs.

A sliding-free boat for multilayer growth has been reported by Scheel [61, 62], which uses a coaxial graphite screw rotating around an horizontal axis. The different liquid solutions are separated by the screw pitches and are transported forward by rotation just as in an Archimedean screw.

2.2 The Sliding Technique

The most frequently used system is the horizontal multi-bin-slider system [2, 63, 29], which enables the growth of multilayered structures. It is the method almost universally used for the growth of heterostructures, e.g. for laser diodes. We will therefore describe this technique in greater detail. In the simplest case the boat consists of a substrate holder with the substrate held in a recess and the slider containing the differently composed solutions in its bins as shown in Fig. 7. As the solution generally do not stick to purified graphite, they can be wiped off the substrate by the graphite walls of the slider to terminate growth. The slider is moved by a horizontal fused silica push rod, which is actuated by hand or, in modern versions, by a computer-controlled stepper motor. The pushing direction is forward and backward, also allowing the growth of multilayers from two neighbouring solutions. Minimum growth times of some tenths of a second per layer are easily achieved [64]. Each solution is usually protected by a graphite cover to prevent evaporation and contamination. Moreover, the covers compress the solutions so that they become geometrically well defined, e.g. cuboidal, so that the diffusional transport is one-dimensional and the "thin-solution" geometry can be realized. In this geometry the solution is surrounded on all six sides by graphite (before the substrate is introduced), which ensures an equal heat transport in all

directions with minimum temperature gradients and minimum convection. Thus, controlled growth conditions are achieved.

Thermal degradation. The sliding boat construction also allows an efficient protection of the substrate against thermal degradation during the heat-up time before growth is initiated. Such a protection is indispensable, for instance, for an InP substrate. It can consist of an InP-Sn solution [65], which evaporates phosphorus through the holes of a graphite basked positioned directly above the substrate surface. An improved version employs an InP-Sn-In solution with excess InP, where the necessary P vapour pressure is controlled by the Sn/In ratio [66]. However, it has been shown that at higher temperatures a Sn-rich solution in a basket can cause a Sn contamination at the substrate-epilayer interface [67-69]. Therefore, a protection using a cover substrate at a distance of less than $100\,\mu m$ from the substrate is preferable for the growth of high purity layers [68, 69]. (111)B-oriented InP cover substrates are best suited since they evaporate markedly more phosphorus than (111)A- or (100)-oriented substrates.

Substrate fixing. When the solution is pushed over the substrate, the latter might float upwards because its specific density is less than that of the solution. In most boat constructions the substrate is thus fixed in the recess in such a way that the width of the solution chambers perpendicular to the pushing direction is smaller than the substrate width. As a consequence, not the entire substrate area is covered by the epilayer, and severe edge growth occurs on these sides. We found that a substrate put into the recess does nor float up even if it is not clamped and the solution overlaps the substrate on all four sides [70]. The substrate can even be smaller than the recess. This fact greatly facilitates the process because now substrates of any shape may be employed, and the whole substrate area is covered by the epilayer. Moreover, more than one substrate can be put into one recess without being clamped. In this way simultaneous growth is possible on substrates which differ, for instance, in their doping, orientation or defect density.

Edge growth. Enhance layer thickness at the edges of the substrate is a severe problem in LPE. Edge growth can amount to a multiple of the average layer thickness [71]. It is caused by the following effects:

1) Thermal convection,
2) an orientation-dependent growth rate at the substrate edge, where different lattice planes are exposed,
3) two-dimensional diffusion of material from the surrounding volume of solution,
4) growth effects related to the surface tension of the liquid. The first effect increases with an increasing cooling rate [72] and is a minimum for isothermal growth. The second effect vanishes if the solution is smaller than the substrate. The third effect can be minimized by the thin-solution technique [72]. As mentioned above, the solution chamber can also be made larger than the substrate recess as shown in Fig. 8a. We found that a solution (3 mm in height) overlapping the substrate on all four sides by
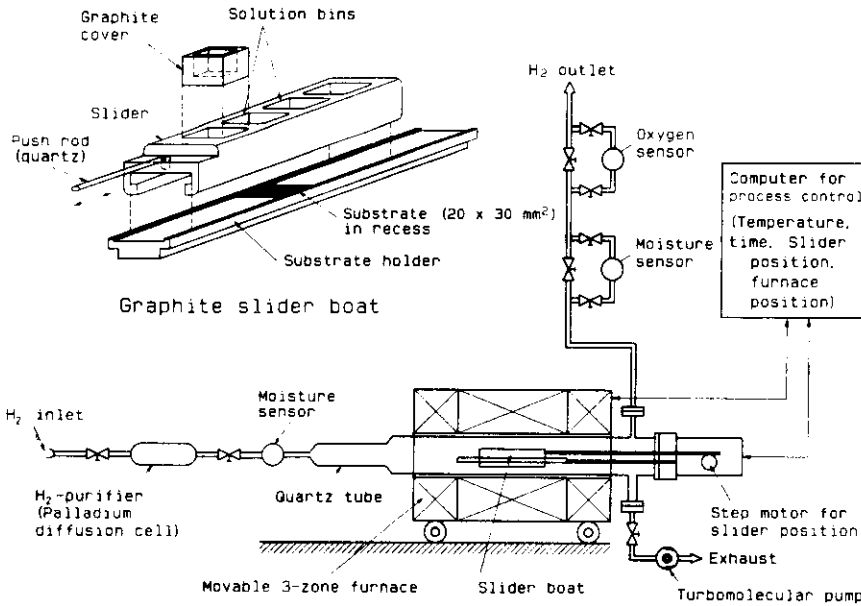
- 11 -

Fig. 7. Schematic view of a horizontal multibin-slider LPE system, after Kuphal [70]
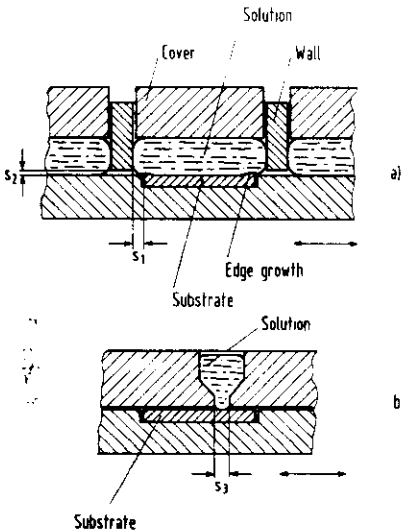

Fig. 8. (a) Details concerning edge growth and solution carry-over in a multibin-slider boat. (b) Slider boat for the production of extremely thin layers according to Alferov et al. [75]

$s_1 = 0.8$ mm produces a minimum of edge growth [70] due to the effects (2) to (4).

Solution carry-over. The crucial point in a sliding boat is the slit s_2 between the substrate surface and the walls of the slider (Fig. 8a). If the slit is too large, solution is carried over into the following chamber, and the composition of subsequent solutions is altered. Solution carry-over not only depends on s_2, but also on the solution height and the push speed [73]. If the slit is too small, the graphite or crystalline particles will cause scratches on the surface of the grown layer in the sliding direction. The problem becomes even more severe when thick layers

with considerable edge growth are deposited. Depending on the contact angles of the solutions used [74] and the thickness of the edge growth, the LPE worker has to optimize the slit height s_2, which may range between 20 and 100 µm. In any case a small tolerance in substrate thickness of ± 10 µm is mandatory.

A drawback of the sliding technique is the relative motion of graphite parts causing abrasion of particles, which can lead to growth defects. Particle abrasion is, however, almost entirely supressed by the use of very hard, low porosity, high density types of graphite (e.g. Poco graphite) [57] or of graphite covered by pyrolithic carbon or boron nitride.

Extremely thin layers in the range of a few nm can be grown by means of the sliding technique if the width of the solution chamber s_3 is small compared to the width of the substrate [75] as shown in Fig. 8b. The growth time is then the ratio of s_3 to the push speed. The sliding boat system has also been extended to the simultaneous growth of multilayers onto several substrates for commercial production [76, 77]. Figure 9 shows a construction used by Heinen [76], where 16 substrates, 15×15 mm^2, stand vertically side by side in successive cavities of 8 substrate holders. Each solution is cut into equally composed thin solutions by the substrate holders. The quality of the epitaxial wafers has been claimed to be equivalent to those of a conventional single wafer system.

Instead of horizontal translatory sliding systems, rotating sliding devices have also been used for multilayer growth [78, 79]. There, the rotation axis and the furnace are arranged vertically. These systems offer advantages for high-speed (thin-layer) applications, but problems arise with the flatness of the temperature profile.

Another promising approach is the centrifugal LPE technique of Bauser et al. [80]: Rapid rotation of the crucible about a vertical axis ensures fast transport of the solutions by centrifugal forces and produces brief contact
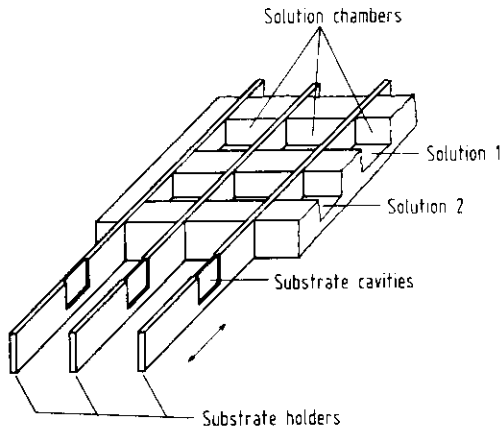
Fig. 9. Principle of a multislice boat for the growth of multilayers, after Heinen [76]

Fig. 10a–d. Different techniques to control the supersaturation. (a) Conventional single-phase solution, (b) two-phase solution, (c) single-phase solution saturated by a source substrate, (d) single-phase solution cut from a larger two-phase solution

between solution and substrate. Thin GaAs and Si n-p-n multilayers have been grown on 12 cm² substrates, but no devices have been produced by this method so far. The method is presently being extended for growth on a 4 inch wafer.

2.3 Single-Phase and Two-Phase Solution Technique

In practice, LPE growth is realized from either a single-phase or a two-phase solution. A single-phase solution (Fig. 10a) is a liquid supersaturated so little that no spontaneous nucleation takes place before the seed substrate is introduced. A two-phase solution is defined here as a solution containing a floating source substrate which is partially dissolved to saturate the solution and which remains present during growth on the seed substrate (Fig. 10b). (In earlier works the term two-phase solution was also applied to the case when a solution is so strongly supersaturated that spontaneous nucleation happens before growth on the substrate is initiated. But layers grown in this mode reveal a rough morphology [35], and, consequently, this method is no longer applied nowadays). The characteristics of the two-phase solution technique are:

1) Less knowledge about the phase diagram is necessary because the solution automatically dissolves the amount of source material required for saturation.

2) If the source substrate covers the whole solution, evaporation is inhibited. Moreover, the solution becomes a cuboid without being substantially pressed.

3) Growth takes place on the seed and on the source substrate. The growth rate is roughly equal to that of a single-phase solution of half the height.

4) Binary two-phase solutions can be re-used many times, guaranteeing each time the same growth conditions.

5) The growth rate derived in Sect. 1.2 for a single-phase solution is not applicable to two-phase solutions since the boundary conditions are different. Due to supercooling, a supersaturation ΔT exists at the seed at the beginning of growth ($t = 0$), but $\Delta T = 0$ at the
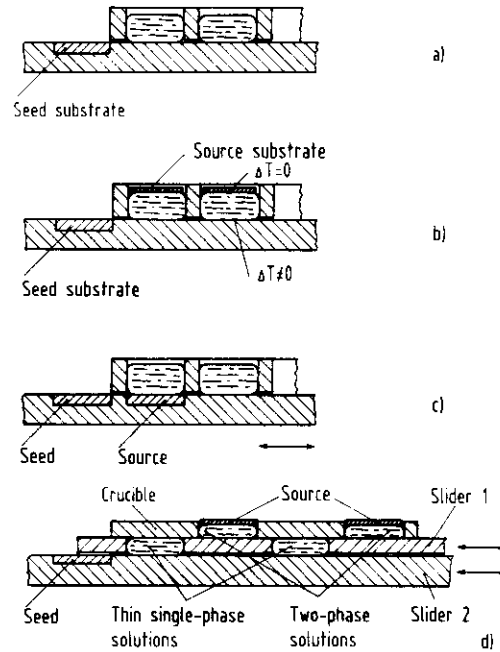
source substrate. Thus, we do not have a homogeneously mixed solution at $t = 0$ but a concentration gradient in the vertical direction, which strongly depends on the temperature-time diagram before $t = 0$. Owing to the sliding motion at $t = 0$ the solution is partially rotated, changing the initial concentration distribution in a way which can hardly be treated theoretically.

The control of the layer thickness d is one of the crucial points in LPE. We will now compare the capabilities of the single-phase and two-phase solution techniques to control d. According to (27), d is proportional to $\Delta T \sqrt{t}$ for short growth times t. While t can be well controlled in automatic systems, the supersaturation $\Delta T = T_s - T_G$ is difficult to control. This is due to the fact that ΔT is a small difference (a few Kelvin) between two incommensurable quantities, namely the saturation temperature T_s as given by the liquid composition, and the actual growth temperature T_G. Incomplete mixing of the solution can change T_s at the phase boundary. Moreover, evaporation loss of volatile elements (e.g. P, Hg, Cd) during the prebake time can noticeably lower T_s.

Using a single-phase solution, the following possibilities exist to control the saturation temperature:

1) Accurate weighing of the source components is the most common and easiest way, but it is hardly accurate enough for the reproducible production of thin-layer device structures.

2) Saturation of the solution by a source substrate at constant temperature in a separate run is accurate but time-consuming.

3) Saturation by the same substrate, which is then used for growth in the same run, results in an inferior

surface morphology, because any melt-back of a substrate causes a wavy and pitted surface.

4) Use of a source substrate for saturation followed by a seed substrate for growth (Fig. 10c). In this arrangement the time for saturation of a solution is determined by the growth time under the next solution, which may be too short. In addition, the danger of melt carry-over is increased if two substrates are slid.

5) Formation of thin single-phase solutions by cutting from larger two-phase solutions by a second slider (Fig. 10d). This is an ideal method to produce homogeneous single-phase solutions with a well-defined saturation temperature, avoiding the disadvantages of floating substrates on the growth solutions. The implementation is, however, rather complicated since two sliders have to be actuated, and the boat has twice the length of a conventional one.

6) Melt casting in a separate furnace: Here, multiple specimens of equal composition are cast from a large-volume solution [81].

In two-phase solutions (Fig. 10b), ΔT at the seed substrate and thus the layer thickness can be well controlled. However, in some heterostructures like InGaAsP/InP, a back-dissolution of the already grown layer is caused by the liquid solution of the next layer, which can only be inhibited by a large ΔT. As ΔT is generally smaller in two-phase than in single-phase solutions, the former technique is problematic in these applications.

3. Growth Properties

3.1 Layer Morphology

As LPE is a near-equilibrium process, the surface mobility of the atoms during incorporation is high and we observe a pronounced lateral microscopic growth [82]. The layer morphology is very sensitive to the properties of the substrate (interface) such as defects and the crystallographic orientation. The misorientation of the interface determines the density of growth steps. If the misorientation to a low-index face is $\leq 0.1°$ and the dislocation density is low, a microscopically flat surface can be obtained with parallel and equidistant growth steps of one monolayer in height. For larger misorientations, however, the monosteps become so dense that they will develop bunches during their lateral motion. The layer surface then shows the well-known growth terraces [56], which are undesirable for devices. Dislocations in the substrate act as sources of monosteps. If the dislocation density is high, these monosteps interfere with each other and cause a macroscopically flat surface without misorientation steps. An example is shown in Fig. 11.

If a substrate with $< 0.1°$ misorientation is used, the obtained microscopically flat surface, the so-called facet, has a diameter of up to a few millimeters limited by a large step. Such a surface is unsuitable for devices. In practice, we use (100)-substrates misoriented by $< 0.1°$ in the $\langle 01\bar{1}\rangle$-direction and by $0.5°$ in the $\langle 011\rangle$-direction. By this trick bunched misorientation steps of moderate step height (≈ 20 nm) parallel to a cleaving direction are
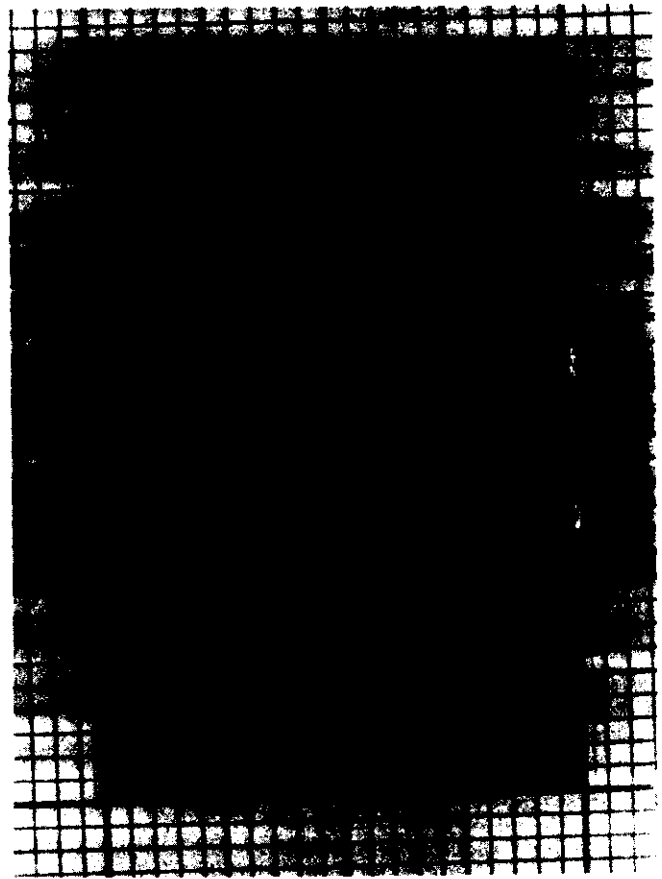

Fig. 11. Macroscopically flat InGaAsP layer (1 µm thick) of seize 20×30 mm^2 grown by LPE at $T = 600°$ C, after [70]
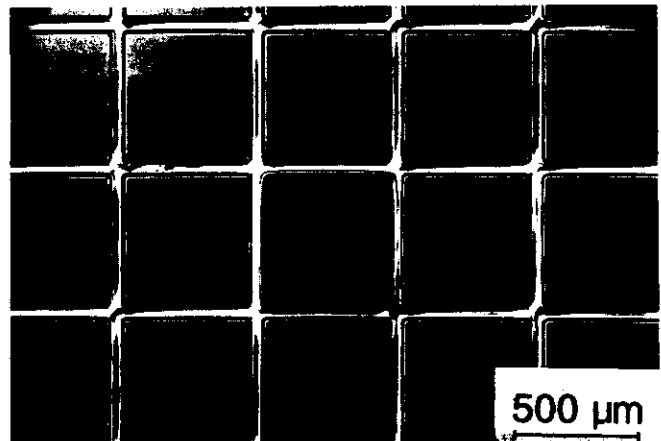

Fig. 12. Facets in a GaAs layer obtained on a square patterned substrate, after [83]

created. Devices such as lasers can be structured on the terrace treads parallel to the steps so that the growth steps cannot affect the device performance.

Another method of obtaining flat surfaces was reported by Morlock et al. [83], who etched a square pattern of lines on a well-oriented substrate producing a grid with squares of 1 mm^2. After growth, microscopically flat facets had covered the squares; see Fig. 12. This way the otherwise unpredictable boundary of the facets
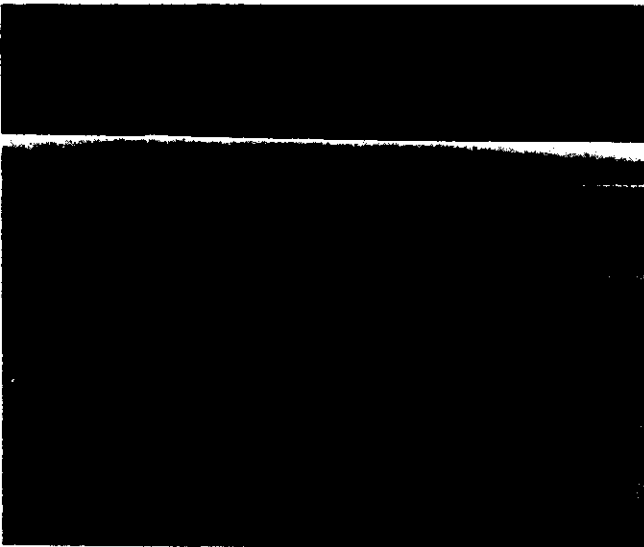
Fig. 13. A groove fully planarized by an AlGaAs/GaAs/AlGaAs layer sequence, after [70]

was forced into the etched boundaries of the squares. Devices can then be positioned into these squares.

3.2 Growth on Structured Substrates

The unique properties of LPE growth on non-planar substrates have a great impact on devices. From the large number of publications on non-planar growth two basic properties can be extracted: Planarization and orientation-dependent growth rate.

1) Due to the lateral microscopic growth, grooves and mesas can be planarized by the growing layer. The planarization of a very deep ($4\,\mu m$) V-groove in GaAs is shown in Fig. 13. A much finer pattern is shown in Fig. 14: A planar InGaAsP DFB $\lambda = 1.53\,\mu m$ laser structure is grown nearly dissolution-free at $T = 600°$ C over a first order grating ($\Lambda = 0.23\,\mu m$) including a $\lambda/4$ phase shift. The depths of the grating before and after LPE growth were 110 nm and 80 nm, respectively [70]. Another example is a planar quaternary heterobipolar transistor (HBT) with buried base. As shown in Fig. 15 the five-layer structure is successfully grown in a two-stage epitaxial process, where the second stage took place on areas both of InP and InGaAsP.

2) Being a near-equilibrium process, the nucleation in LPE is strongly orientation dependent. The relative ease of nucleation of different materials on structured InP has been measured by Chand et al. [84] to be:

InP $\quad\quad\quad\quad$ (100) > (111)B ≫ (111)A

$In_{0.53}Ga_{0.47}As$ $\quad$ (100) ≫ (111)A > (111)B

$In_{0.75}Ga_{0.25}As_{0.55}P_{0.45}$ (100) ≫ (111)B > (111)A.

A whole class of devices is based on the fact that the growth rate on (111)-oriented mesa edges is lower than on the (100)-plane, for instance V-groove lasers and various forms of buried heterostructure (BH) lasers with infill layers.
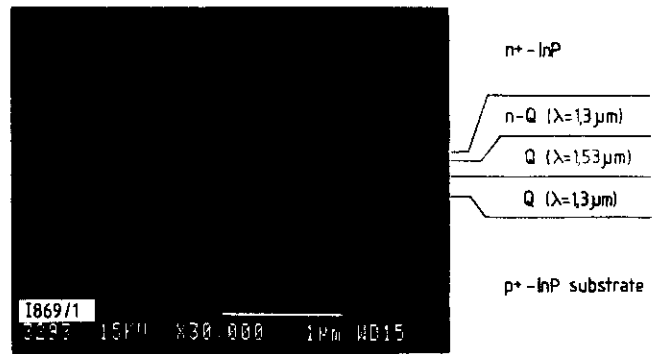

Fig. 14. InGaAsP DFB laser structure grown nearly dissolution-free over a first order grating, after [70]. For details, see text
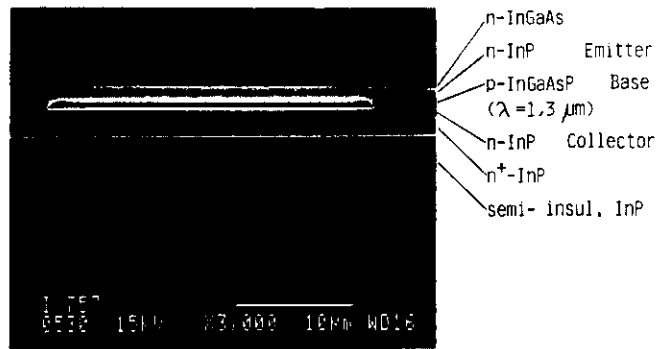

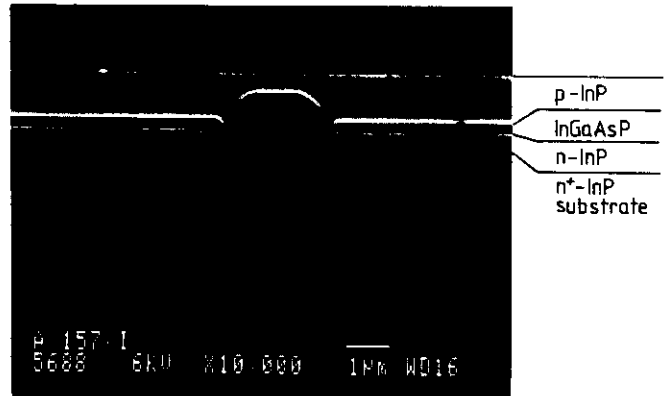Fig. 15. Buried base planar HBT structure, after [70]

Fig. 16. Laser structure ($\lambda = 1.3\,\mu m$) with $2\,\mu m$ wide buried active layer grown by a single-step LPE, after [70]

The low growth rate of especially the quaternary material on (111)-oriented mesa edges allows the growth of BH lasers even by a single-step LPE, as is depicted in Fig. 16: On a patterned substrate with mesas along the $\langle01\bar{1}\rangle$-direction an InP/GaAsP/InP layer sequence is grown in such a way that the thin buffer layer covers the whole mesa but does not planarize it, the quaternary layer is interrupted at the edges and the top layer planarizes the structure. This way the buried active layer is produced without growth interruption which facilitates the process and is advantageous with respect to laser lifetime. This novel structure cannot be grown by any other epitaxial technique.

Table 1. Reproducibility and homogeneity of LPE layers, wafer area $30 \times 20 \, mm^2$, after Kuphal [70]

	Standard deviation σ	
	From run to run	Across a wafer
GaAs and InP		
Thickness (at $d = 0.9 \, \mu m$)	7%	10%
Carrier concentration (at $n = 10^{17} \, cm^{-3}$)	10%	3%
$In_{0.53}Ga_{0.47}As$		
Thickness (at $d = 0.4 \, \mu m$)	10%	10%
Carrier concentration (at $n = 10^{17} \, cm^{-3}$)	10%	3.2%
Lattice mismatch $\Delta a^{\perp}/a$	1.5×10^{-4}	0.82×10^{-4}
Composition parameter x	1.1×10^{-3}	6×10^{-4}
Wavelength (at $\lambda = 1.67 \, \mu m$)	2.6 nm	1.4 nm
InGaAsP ($\lambda = 1.3 \, \mu m$ and $1.55 \, \mu m$)		
Thickness (at $d = 0.15 \, \mu m$)	20%	7%
Lattice mismatch $\Delta a^{\perp}/a$	1.3×10^{-4}	–
Wavelength	7 nm	1.4 nm

3.3 Reproducibility and Uniformity

The reproducibility from run to run and the uniformity across the wafer of some layer properties (layer thickness, carrier concentration and alloy composition) have been measured [70] for LPE layers grown in a horizontal sliding boat system of the type shown in Fig. 7. The materials chosen were GaAs, InP, InGaAs and InGaAsP with $\lambda = 1.3 \, \mu m$ and $\lambda = 1.55 \, \mu m$ with thicknesses corresponding to those of laser structures. The standard deviations σ of the respective average values were determined from at least 10 samples in each case and are summarized in Table 1. For the binaries InP and GaAs, single-phase solutions saturated in a separate run and two-phase solutions yielded equally good results, whereas weighing the source components was clearly inferior. For InGaAs only the weighing of the source components could be applied since saturation by a GaAs substrate does not lead to a steady-state two-phase solution. For the two quaternary compositions weighing of the source components and two-phase solutions yielded equal results. The table demonstrates that the thickness control is only moderate; it is more or less independent of the material and gets worse with decreasing thickness. The control of the carrier concentration meets most device requirements, and the control of the solid composition (expressed by its lattice mismatch and gap wavelength) is considered to be very good.

4. The InP/InGaAsP Material System

In this section we describe the LPE growth of the material system InP/InGaAsP as an example of the many materials which can be grown by LPE. This system is chosen because here LPE has particular advantages over competing methods, as is discussed in Sects. 5 and 6.

In the quaternary $In_{1-x}Ga_xAs_yP_{1-y}$ system lattice-matched to InP the range of possible gap wavelengths is

between $\lambda = 0.92 \, \mu m$ (InP) and $1.67 \, \mu m$ ($In_{0.53}Ga_{0.47}As$). InGaAsP is the most important material system for devices of longer wavelength fiber optics. While the growth of P-containing materials by means of MBE is difficult due to the low sticking coefficient of P, LPE and MOVPE are well suited for the growth of InP based materials. In the InP/InGaAsP system, unlike in GaAs/GaAlAs, lattice matching is only achieved by a precise control of the composition parameters x and y given by (73–74).

The LPE of InP, InGaAs and InGaAsP is generally performed at temperatures between 550 and 650° C. At high temperatures the danger of thermal degradation of the layers exists, and they have to be protected as described in Sect. 2.2. At low temperatures problems arise with the immiscibility region in the alloy systems InGaAs and InGaAsP.

4.1 InP

InP is generally grown from In solutions, but also from Sn solutions for certain applications. Figure 17 shows the phase diagrams of both systems [66]. They can be approximated by the two exponentials quoted in the figure. The phase diagram of the general case In–P–Sn is given in Fig. 18. It is seen that the solubility of P is almost constant between $x_{Sn} = 0$ and 0.5, but increases rapidly towards high Sn mole fractions. The data are well reproduced by the regular solution model (58–62) using the interaction parameters α(In–P), α(P–Sn) and α(In–Sn) as quoted in the figure. The exponential function given in Fig. 17 for the solubility in the binary In–P system is easily deduced by inserting the value of α(In–P) into (50). Figure 17 demonstrates that the solubility of P in Sn is much larger than in In. Hence, the same growth rate is achieved from Sn solutions at much lower temperatures (450–500° C). Growth of InP from Sn solutions allows the following applications:

1) Growth of strongly n-doped ($3 \times 10^{19} \, cm^{-3}$) InP.

2) If InP is grown from an In solution over InGaAs or longer wavelength InGaAsP, a meltback of this layer is observed. This meltback is generally avoided by the insertion of an anti-meltback layer of intermediate composition. Meltback can, however, also be minimized if the InP is grown from a Sn solution [85] due to the higher growth rate and lower temperature. This method has successfully been applied to the growth of $\lambda = 1.54 \, \mu m$ InGaAsP and $\lambda = 1.66 \, \mu m$ InGaAs lasers without anti-meltback layer [86].

3) The same advantage applies for the growth on structured layers: The grating in the InGaAsP layer of DFB lasers can be overgrown by InP from Sn solutions almost dissolution-free [87], which is not possible from In solutions.

The layer thickness of InP grown from In solutions is shown in Fig. 19 for short growth times [70]. The curve fits very well the $\sqrt{t}$-law for step-cooling according to (27). A layer thickness of only 35 nm is achieved with $t = 0.3 \, s$ in an automated LPE growth system.

Layer purity. The Hall mobility versus electron concentration curves at room temperature (RT) and $T = 77 \, K$
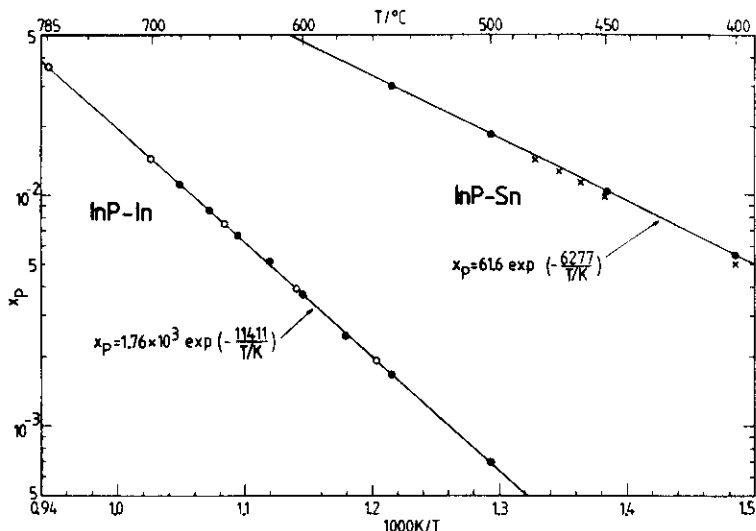
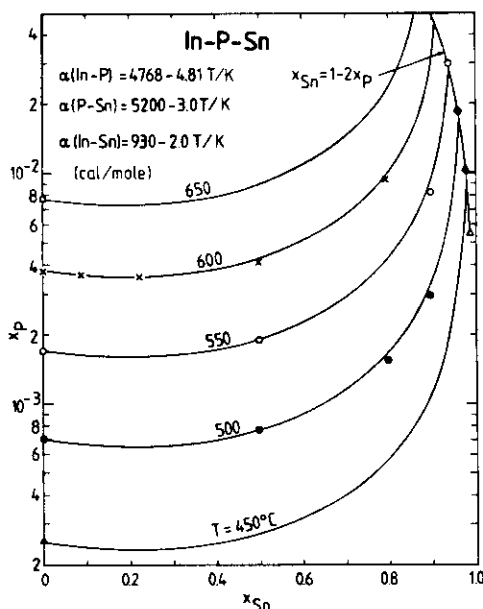Fig. 17. Solubility of phosphorus in solutions of InP in In and InP in Sn. (×) from [85], (o) from [51], (•) from [66]

Fig. 18. Phase diagram of In–P–Sn between $T = 450°$ C and $650°$ C. The full lines denote model calculations [66]
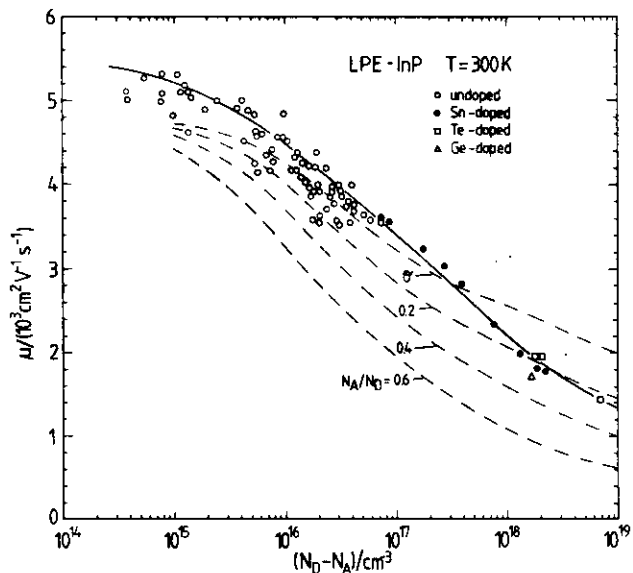

Fig. 20. Hall mobilities at RT of LPE InP layers as a function of carrier concentration [88]. Solid curve: Experimental "universal" mobility curve. Dashed curves: Theoretical drift mobilities [89]
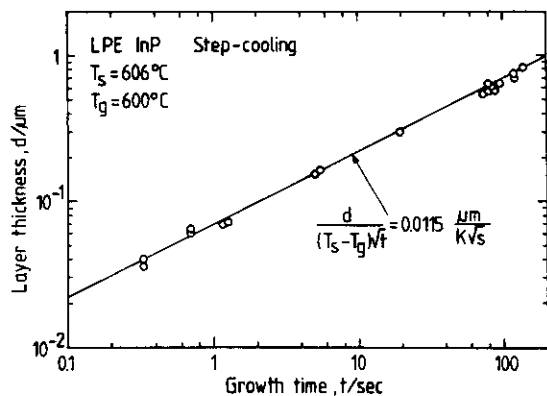

Fig. 19. Layer thickness of InP versus growth time [70]

of LPE InP are shown in Figs. 20 and 21, respectively [88], and compared to the theoretical drift mobility curves of Walukiewicz et al. [89]. Layers grown from nominally undoped In solutions are n-type, due to the presence of S and Si [90] in the In-source. These impurities have large distribution coefficients in InP [91]. By long-term prebaking of the solutions background carrier concentrations of 4×10^{14} cm^{-3} and mobilities $\mu(296\ \mathrm{K}) = 5300$ cm^2/Vs and $\mu(77\ \mathrm{K}) = 75000$ cm^2/Vs have been achieved [88]. Nominally undoped LPE InP is essentially free of deep levels: It contains only two electron trap levels with concentrations below 10^{14} cm^{-3} and no hole traps at a detection limit of 10^{13} cm^{-3} [92].

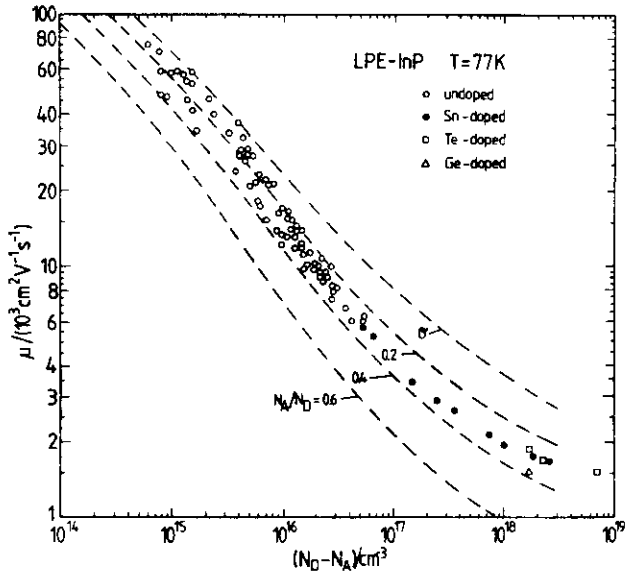*Doping.* The n-type dopants Sn, Ge, Si, Te, Se and S and the p-type dopants Zn, Cd, Mg and Be have been

Fig. 21. Hall mobilities at $T = 77\,K$ of LPE InP layers as a function of carrier concentration [88]. Dashed curves: Theoretical drift mobilities [89]
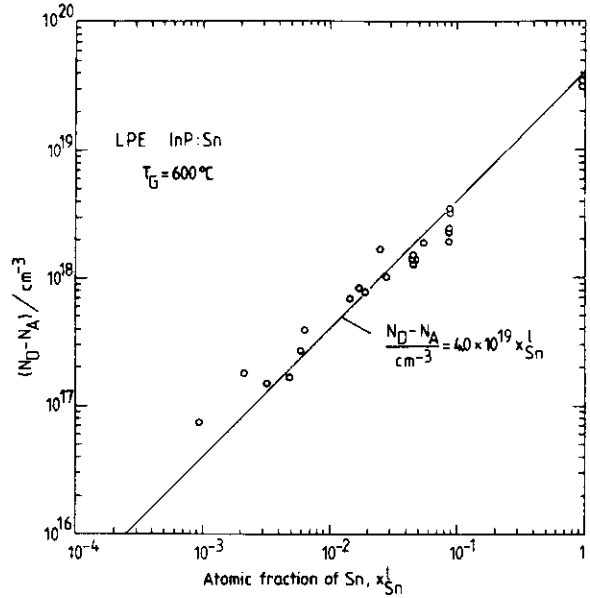
Fig. 22. Carrier concentration in InP grown from Sn-doped In solutions up to the limit of a pure InP–Sn solution [66]

used in the LPE of InP. The results for vapour pressure, distribution coefficient, diffusion coefficient and activation energy are collected in [29, 91, 93]. In practice, Sn is the most commonly used donor dopant in InP due to its low distribution coefficient, high solid and liquid solubility, and low vapor pressure. Its incorporation in InP is shown in Fig. 22. For p-type doping, Zn is usually used, allowing hole concentrations up to $3 \times 10^{18}\,cm^{-3}$ [91, 93]. At moderate doping levels ($p < 1 \times 10^{18}\,cm^{-3}$) almost no outdiffusion of Zn occurs during growth. From post-growth annealing studies we have clear evidence that Zn incorporated in InP by LPE diffuses much less than Zn incorporated by ampoule diffusion does [70]. This

means that Zn occupies different lattice sites in these two processes.

The growth of semi-insulating InP by Fe-doping is only possible at temperatures above $850°\,C$ [94]. At these temperatures, however, the layers are severely corroded by thermal attack, inhibiting in practice the production of semi-insulating InP:Fe by LPE.

4.2 InGaAs

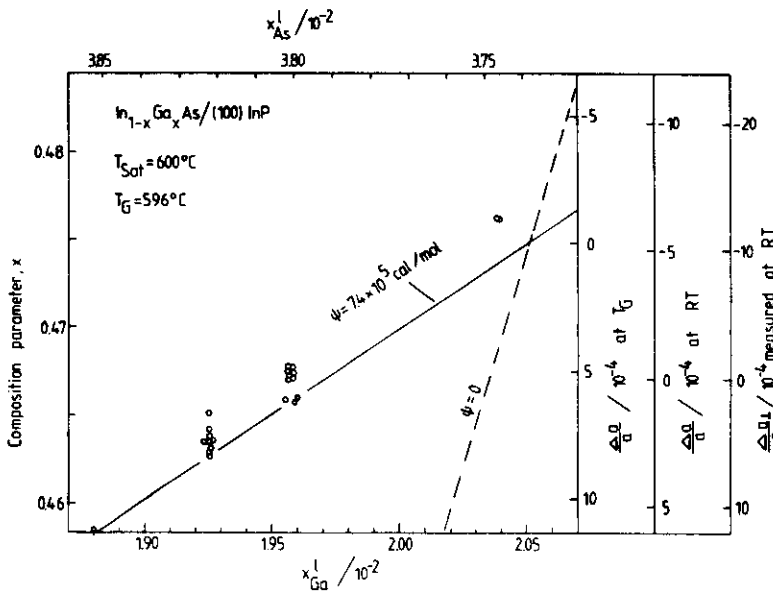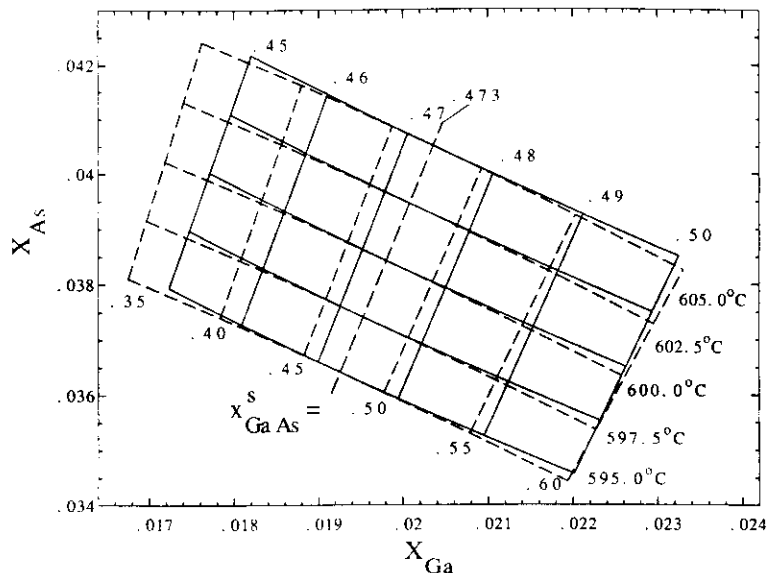The phase diagram data as a function of temperature for lattice-matched growth of InGaAs on (100)-InP have

Fig. 23. Compositions of $In_{1-x}Ga_xAs$ layers grown from different liquid compositions belonging to the same isotherm (600° C). The difference between the data and the dashed curve demonstrates the lattice-pulling effect [64]

Fig. 24. Solid-liquid phase diagram of $In_{1-x}Ga_xAs$ near $T = 600°$ C. Indicated are isotherms and isoconcentration lines corresponding to the "free" phase diagram (dashed lines) and to the strained diagram (solid lines) for growth on (100)-InP [33]

been summarized by Kuphal [45]. Moreover, the phase diagram should also correctly predict the growth of mismatched compositions. Figure 23 shows how the composition parameter x varies for growth from different In–Ga–As solutions, which all have the same saturation temperature T_s and growth temperature T_G [64]. Here, x was determined by measuring the lattice mismatch by means of X-ray diffraction. The ordinates indicate the relations between four quantities, namely the measured mismatch $\Delta a^{\perp}/a$ of the tetragonally distorted epitaxial layer, the mismatch $\Delta a/a$ of the relaxed cubic layer at RT, the mismatch at T_G, and the composition x. The dotted and the solid lines show the dependence of x on liquid composition calculated from (58–62) without ($\psi = 0$) and with strain energy, respectively, using the parameters of Ref. [33]. Good agreement is found between the data and the solid line, although it has not been adjusted. The strain energy follows from the elastic constants of InGaAs and (55) without any free parameter.

The values of x in Fig. 23 obviously depends much less on the liquid composition than expected from the regular solution model without strain. This behaviour is called the lattice-pulling or composition-latching effect, which is demonstrated here for the system InGaAs on (100)-InP. It has also been found for the LPE growth of InGaAs on (111)B–InP by Takeda and Sasaki [95] and of InGaP on GaAs by Stringfellow [96]. The lattice-pulling effect facilitates the control of the lattice-matched composition and is therefore an advantage of LPE over MBE and MOVPE, where this effect does not exist.

The solid-liquid phase diagram of the In-rich part of the system In–Ga–As near $T = 600°$ C is given in Fig. 24. The isotherms and isoconcentration lines of the "free" phase diagram are compared to the strained phase diagram for growth on (100)-InP. At the composition of lattice match ($x = 0.473$ at $T = 600°$ C) the two diagrams coincide. The figure demonstrates the dramatic widening of the solidus lines caused by the strain energy. Figure 25 shows the "realistic" phase diagram in an x versus

x_{Ga} plot for the growth of $In_{1-x}Ga_xAs$ on InP over the entire range of compositions [64], again using the parameters of Ref. [33]. In the vicinity of lattice-matching we observe the lattice-pulling effect (with flat slopes of the curves), while for larger mismatches the strain energy is relaxed by the formation of misfit dislocations [97] and, therefore, the normal unstrained phase diagram is again valid. The transition between the two regions is described mathematically by a Gaussian for the strain energy factor $\psi(x)$ as indicated in the figure.

For a given liquid composition, i.e. fixed T_s, the alloy composition depends markedly on the growth temperature T_G, as shown in Fig. 26 [33]. This dependence is given by (33). Inserting the respective phase diagram values and derivatives, adjustment of (33) to the data of Fig. 26 yields the ratio of the diffusion coefficients $D_{Ga}/D_{As} = 0.42 \pm 0.09$.

Growth rate. The layer thickness of lattice-matched InGaAs in the range 0.2–5 μm is plotted in Fig. 27 as a function of growth time for a fixed supersaturation and cooling rate [64]. The data closely follow equation (30) valid for supercooling with the constant $K(600°$ C$) = 0.069$ μm/(K$\sqrt{s}$). Using this value of K and the ratio D_{Ga}/D_{As} obtained from Fig. 26, equation (26) allows the separate computation of the two diffusion coefficients carried out in Ref. [33]. In this way the LPE process of InGaAs including the phase diagram and the diffusion law is described completely.

Layer purity. The degrees of purity of LPE InGaAs achieved by different authors [88, 98–100] are demonstrated in Fig. 28 by the Hall mobilities at RT and $T = 77$ K as a function of carrier concentration. The purest samples have a background doping in the low 10^{14} cm^{-3} range and mobilities of 13000 and 70000 cm^2/Vs at RT and 77 K, respectively. The crystalline perfection of LPE InGaAs is further proved by the linewidths of the rocking curves in Fig. 29 [64]. The figure shows examples of positive and negative lattice mismatch measured by Cu $K_{\alpha 1}$
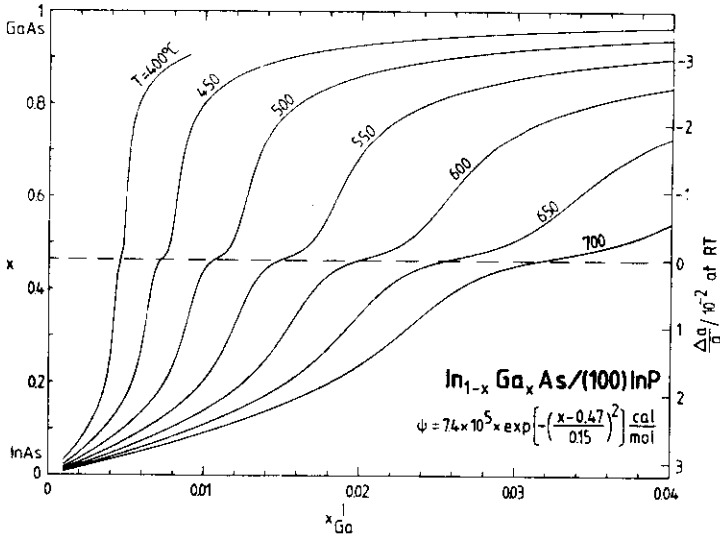
Fig. 25. Phase diagram of InGaAs for the growth on InP between 400° C and 700° C over the entire range of compositions [64]
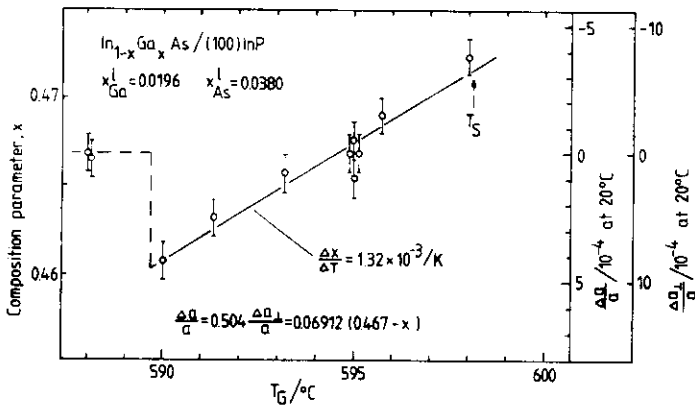

Fig. 26. Dependence of solid composition (or lattice mismatch) of InGaAs on the supersaturation $T_s - T_g$ [33]
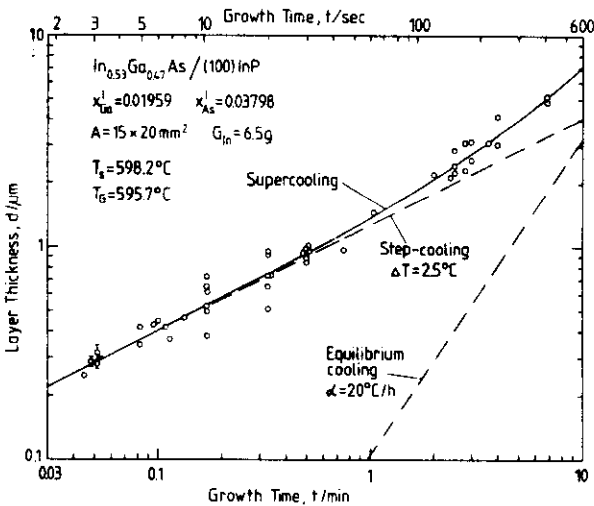

Fig. 27. Layer thickness of InGaAs as a function of growth time [64]

radiation under (400)-reflection. The best value of the linewidth found is 16″. This small value also shows that this layer is practically free of compositional grading, although it is rather thick (4.2 μm). This linewidth is the smallest measured for LPE InGaAs so far.

Doping. Sn is usually employed as dopant for the n-doping of InGaAs; and Zn or Mn for the p-doping. Figure 30 shows the incorporation of Sn in InGaAs up to $x_{Sn} = 0.50$ [64]. The relation between n and x_{Sn} is very similar to that for Sn in InP, see Fig. 22; therefore, the distribution coefficient $k_{Sn} = 2.0 \times 10^{-3}$ [91] holds for both systems. For p-doping of InGaAs, Zn is favoured due to its small activation energy $E_A = 22$ meV [101]. As is summarized in Fig. 31, hole concentrations between 5.5×10^{15} cm^{-3}, achieved by careful overcompensation of the n-type background [88], and $p = 2 \times 10^{19}$ cm^{-3} [102–105] have been published. Mn also forms a fairly shallow acceptor ($E_A = 45$ meV) in InGaAs [106], and hole concentrations between 4×10^{15} and 3.5×10^{18} cm^{-3} have been achieved [106–108]. In InP and InGaAsP, however, Mn is a much deeper acceptor, which excludes its use for p-type layers.

4.3 InGaAsP

The phase diagram of InGaAsP has already been discussed in Sect. 1.3.3. Various cuts through this four-dimensional phase diagram are given in [31, 45, 50]. As an example, Fig. 32 shows the dependence of the liquid atomic fractions x_{Ga}, x_{As} and x_P on the solid As com-
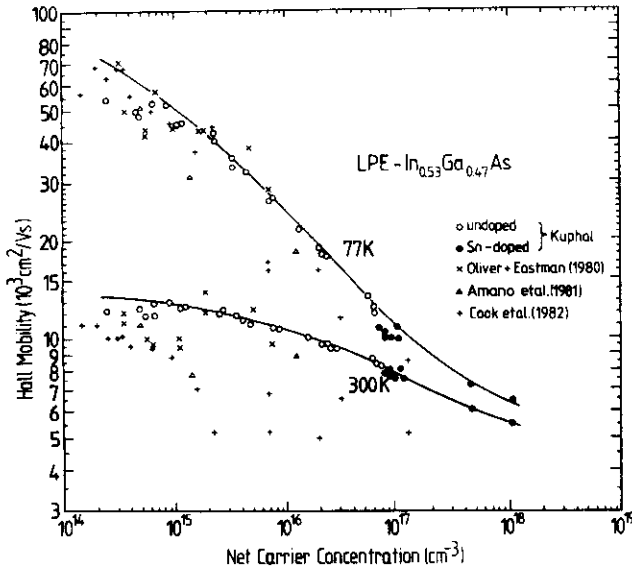
Fig. 28. Hall mobilities at $T = 300\,K$ and $77\,K$ of InGaAs as a function of carrier concentration [88, 98-100]. The solid curves represent averages through the best data
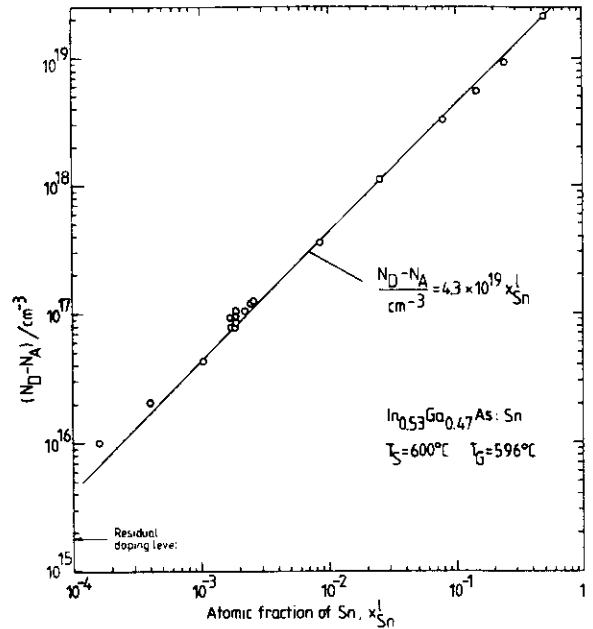

Fig. 30. Carrier concentration of InGaAs grown from Sn-doped In solutions up to $x_{Sn} = 50\%$ [64]. At high Sn concentrations in the liquid the phase diagram considerably depends on x_{Sn} [54]

position parameter y of lattice-matched compounds at $T = 600°\,C$ [45]. The curves demonstrate that good control of the solid composition over the entire composition range is possible be means of LPE.

Miscibility gap. In some ternary and most quaternary III–V systems a miscibility gap exists [109] in the sense that at certain liquid compositions and temperatures no equilibrium with a single solid phase exists, but two solid phases with different compositions are created. For In-GaAsP a miscibility gap has been predicted theoretically by de Cremoux et al. [110], Onabe [109, 111] and Stringfellow [112, 113]. In Fig. 33 the miscibility gap is presented in a temperature versus composition diagram [45] based on the parameters of Onabe [111]. According to this curve it is only at high temperatures ($> 681°\,C$)

that all compositions $y = 0$–1 can be grown. Phase separation in epilayers can experimentally be detected by (1) a broadening of the photoluminescence (PL) or (2) a broadening of the X-ray linewidth, (3) reduced electron mobility, (4) limited attainable layer thickness [45, 114], and (5) direct observation by TEM [115]. The data points in Fig. 33 reveal that single solid phase layers can nevertheless be grown within the predicted miscibility gap. The effective miscibility gap valid for growth of InGaAsP on InP is obviously smaller, as indicated by the dashed line. This deviation is explained by the fact that the substrate strain energy stabilizes the growing solid to some extent. This effect is not contained in the theory of Ref. [111].
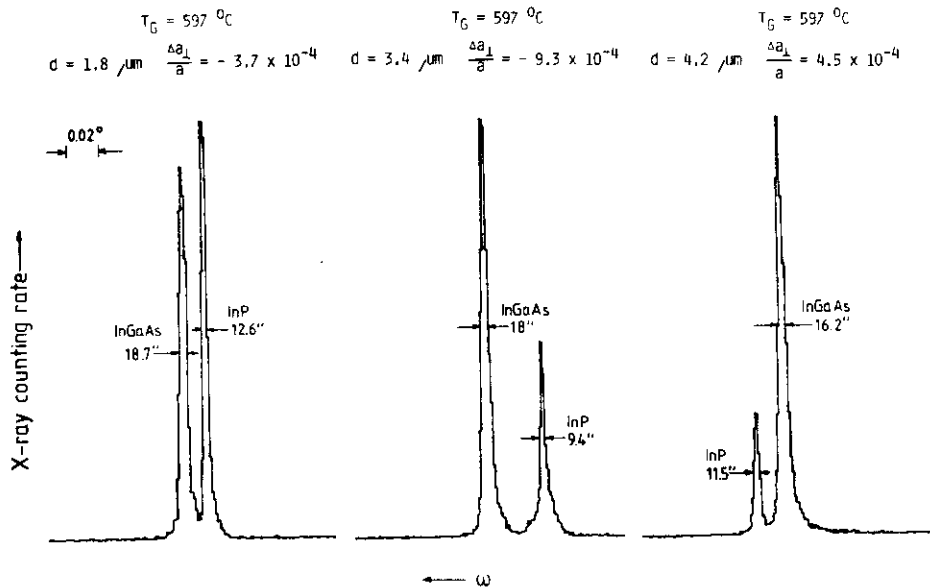

Fig. 29. X-ray rocking curves of different InGaAs samples. The layer thickness, the lattice mismatch and the linewidth (FWHM) are indicated for each sample [64]
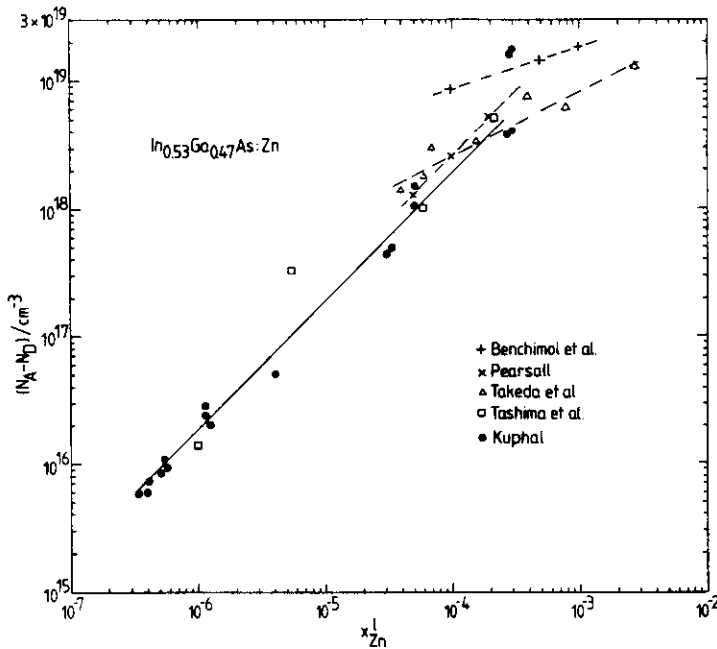
Fig. 31. Hole concentrations at RT of InGaAs layers as a function of the atomic fraction of Zn in the liquid [88, 102-105]. At low Zn concentrations $N_A - N_D$ is proportional to x_{Zn} with $k_{Zn} = 0.65 \pm 0.07$
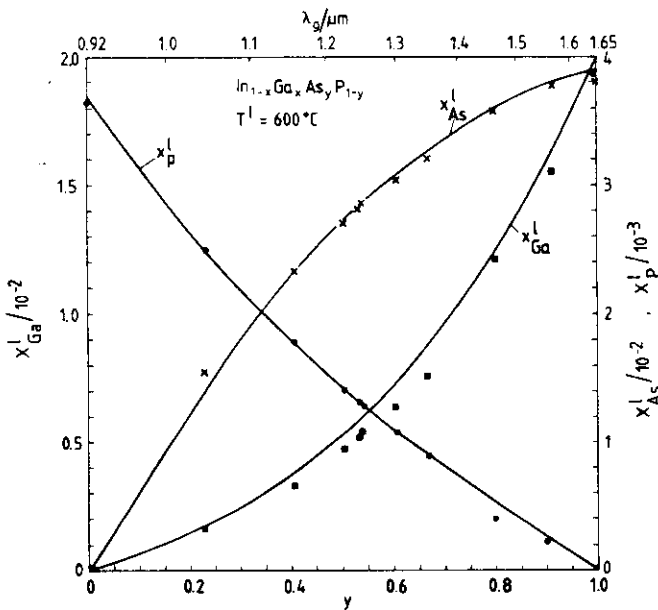

Fig. 32. Atomic fractions of As, Ga and P in the liquid versus As content in InGaAsP, and gap wavelength λ_g [45]. The data agree with the phase diagram (solid lines) using (66-71)

As an example of how phase separation can be detected, Fig. 34 shows the PL linewidth of InGaAsP layers over the whole composition range. While pure layers ($n < 3 \times 10^{15}\,\mathrm{cm}^{-3}$) grown at $T = 630°\mathrm{C}$ yield linewidths of about 10 meV at $T = 10\,\mathrm{K}$, layers with the same purity deposited at 595°C exhibit a dramatic linewidth broadening in the composition range expected for phase separation around $\lambda = 1.4\,\mu\mathrm{m}$, but normal linewidths outside this region. A further indication for phase separation is the reduced electron mobility as a result of enhanced alloy scattering. Figure 35 shows a comparison of 77 K Hall mobilities as a function of y with the growth temperature and carrier concentration as parameters [45]. The mobility of high purity material grown at 630°C [116] reveals a minimum at the expected center of the misci-

bility gap ($y \approx 0.7$), while layers of comparable purity grown at 685°C [117] or 740°C [118] yield substantially higher mobilities in the range $0.55 \leq y \leq 0.9$. Outside this range the mobilities for equal carrier concentration are essentially independent of growth temperature. This again demonstrates that the miscibility gap can be overcome at higher temperatures.

Growth rate. The thicknesses of thin lattice-matched InGaAsP ($\lambda = 1.28\,\mu\mathrm{m}$) layers grown under supercooling conditions are given in Fig. 36 as a function of growth time t. As expected, the curve follows the $\sqrt{t}$-law. The constant K of (26) is $0.0123\,\mu\mathrm{m}/(\mathrm{K}\sqrt{s})$ for this compound at 600°C, indicating that the growth rate of InGaAsP is between that of InP (Fig. 19) and InGaAs (Fig. 27).
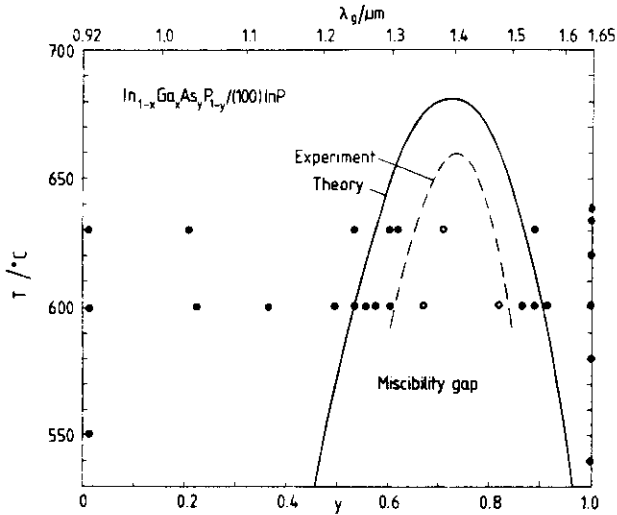
-22-

Fig. 33. Miscibility gap of InGaAsP/InP in a temperature versus composition diagram after Kuphal [45]. The data denote stable (•) and phase separated (o) compositions, from which the realistic extension of the miscibility gap is derived (dashed line). The theoretical curve (solid line) is after Onabe [111]
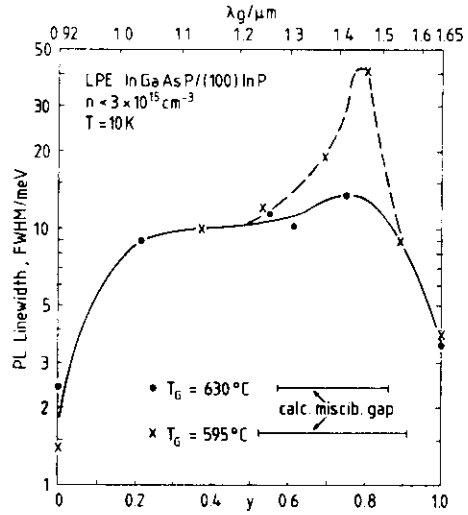

Fig. 34. Linewidths of photoluminescence spectra of InGaAsP as a function of composition [64]. The broadening of the linewidth of certain samples is attributed to the miscibility gap
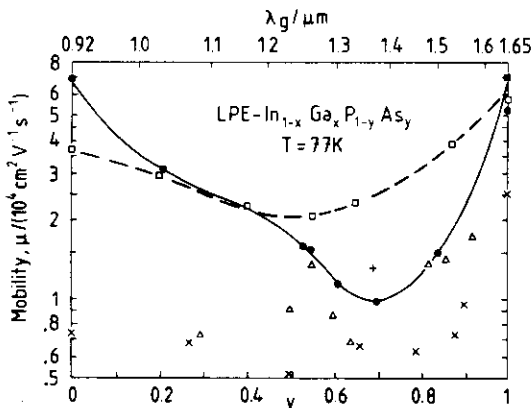

Fig. 35. Hall mobility at $T = 77$ K of undoped InGaAsP/InP versus y with the growth temperature as a parameter [45]

	Reference	$(N_D - N_A)/\mathrm{cm}^{-3}$	$T_G/^\circ$ C
△	[119]	$(1-3) \times 10^{16}$	659
■	[98]	4×10^{14}	650
×	[120]	$\sim 10^{17}$	635
•	[116]	$(0.2-1.1) \times 10^{15}$	630
+	[117]	1.6×10^{15}	685
□	[118]	$(0.6-2) \times 10^{15}$	740

Fig. 36. Layer thickness of InGaAsP as a function of growth time. N denotes the number of samples measured [64]

In the same way the constant K has been determined over the whole InGaAsP/InP system by Kuphal [70]. The results are shown in Fig. 37. The solid curve in this figure has been calculated after (26). The necessary derivations $\partial T/\partial x_i$ have been measured in separate experiments. The diffusion coefficients D_{Ga}, D_{As} and D_P used are indicated in the figure, and they are those determined at InP and InGaAs. Thus, the solid curve in Fig. 37 is not a fit to the quaternary data points and its good agreement with the experiments demonstrates that the growth rate in a system even as complicated as InGaAsP is well understood today.

Layer purity. High purity InGaAsP layers with $n <$ 1×10^{15} cm^{-3} have been achieved by LPE over the entire composition range [116], see also Fig. 35. The room temperature mobilities of these layers reveal a linear dependence on composition between $y = 0(\mu = 5300)$ and $y = 0.7(\mu = 6100)$, and then increase towards the ternary limit $y = 1(\mu = 13000 \,\mathrm{cm^2/Vs})$. Less pure layers exhibit a downward bending of the $\mu(y)$ curve with a minimum between $y = 0.3$ and 0.4 [119, 120].

Doping. N-type doping of InGaAsP is mostly performed by doping with Sn. As the distribution coefficients of Sn in InP and InGaAs are equal (Sect. 4.2), the same value can be expected for InGaAsP, too. This has been proved by Fiedler et al. [108]. The doping behaviour of the p-type elements Cd, Mn, Mg and Zn in InGaAsP has also been investigated in Ref. [108].

-23-

Fig. 37. The constant K for the growth rate after (26) for the complete InGaAsP system. After Kuphal [70]

5. Comparison with competing Methods

The question which epitaxial method is the most promising has many aspects and can only be answered for a specific device application. The essential features of the three most commonly employed epitaxial methods, namely LPE, MOVPE and solid-source MBE, will be discussed in the following using Table 2 as a guide-line. Other methods like VPE, MOMBE, CBE and GSMBE also have specific advantages for certain applications but are omitted here.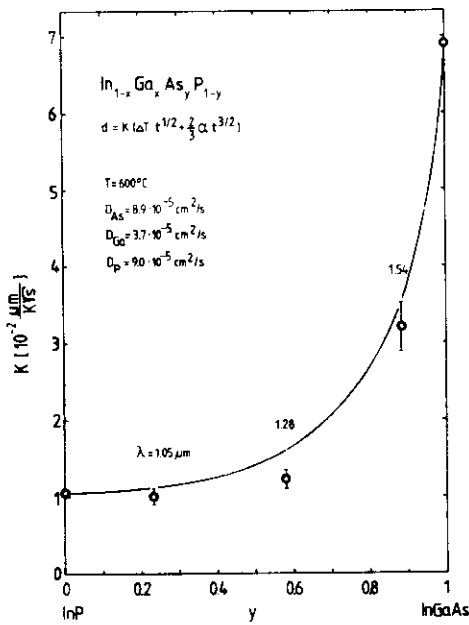 Points (1) to (11) in Table 2 denote advantages of the LPE process, whereas points (12) to (20) describe its drawbacks.

5.1 Advantages of LPE

1) An essential point is that LPE growth takes place near thermal equilibrium between solid and liquid, whereas MOVPE and MBE are non-equilibrium processes. This characteristic of LPE is responsible for the growth correlated material properties labeled (2) to (5) and (13), (15), (16), (20) in Table 2.

2) The achievable bulk layer purity measured electrically and optically is excellent; see also the results in Sect. 4. The mobility values and the outstanding photoluminescence (PL) intensity achieved with LPE samples are often used as standards for other epitaxial techniques. But the other epitaxial methods are also able to yield excellent layer purity. For $In_{0.53}Ga_{0.47}As$, e.g., the narrowest PL linewidths observed are $\Delta E = 2$–3 meV for LPE [101], 1.5 meV for MOVPE [121], and 4 meV for MBE [122].

3) The crystalline quality of binary and ternary compounds as characterized by X-ray diffraction is excellent for all three epitaxial methods. We choose again the example of $In_{0.53}Ga_{0.47}As$: Linewidths of rocking curves under (400)-reflection of 16″ for LPE [64], 16″ for MOVPE [121], and 12.5″ for MBE [123] have been achieved. However, we found that the etch rate by wet chemical etching of MOVPE and MBE InGaAs is about twice that of LPE InGaAs indicating a higher density of point defects in the former materials. Also the dark current of InGaAs pin-photodiodes made of MBE material was an order of magnitude higher than that of LPE material, although the electrical purity of both materials was equal [124].

4) The control of close lattice match in heterostructures such as InGaAs/InP and InGaP/GaAs is very much facilitated in LPE by the lattice-pulling effect (Sect. 4.2 and Table 1), which means that the growing interface incorporates the "right" atoms from the solution. In the other epitaxial methods lattice match is only achieved by a very careful control of the gas flow rates.

Table 2. Essential features of the basic epitaxial techniques

	LPE	MOVPE	MBE
1) Equilibrium process	yes	no	no
2) Layer purity (electrical and optical)	+	+	+
3) Crystalline quality (X-ray)	+	+	+
4) Control of lattice match	+	(+)	(+)
5) Orientation-dependent growth	+	(−)	(−)
6) P-containing compounds	yes	yes	no
7) Deposition efficiency	high	low	low
8) Costs of growth apparatus	low	high	high
9) Costs of safety equipment	low	very high	low
10) Environmental risk	no	yes	(no)
11) Suitability for LED production	+	−	−
12) Suitability for laser production	(−)	+	+
13) Miscibility gap	yes	no	no
14) Strained layer epitaxy	−	+	+
15) Sharpness of heterotransitions (ML = Monolayer)	4–18 ML	1–3 ML	1 ML
16) Back − dissolution	yes	no	no
17) Thin layers (< 100 nm)	(−)	+	+
18) Atomic layer epitaxy	−	+	(+)
19) Thickness control	10%	2%	2%
20) Surface flatness	(−)	+	+

+: advantageous, −: disadvantageous

- 24 -

5) Being a near-equilibrium process, LPE growth is much more sensitive to the substrate orientation than the other epitaxial techniques (Sect. 3.2). Advantage is taken of this property in the LPE production of several InGaAsP/InP DH laser structures such as the buried heterostructure (BH) laser [125], the double-channel planar buried heterostructure (DCPBH laser [126], the V-groove laser [127] and the buried crescent (BC) laser [128]. BH structures can even be produced by a single-stage of LPE process [127, 129]; see also Fig. 16. These laser structures are difficult or impossible to grow by other methods.

6) Phosphorus-containing compounds such as InP can be grown by LPE, MOVPE, CBE and GSMBE, whereas in solid-source MBE their growth is almost impossible. Therefore, MBE is unsuitable for the whole field of InGaAsP/InP fiber optic devices. In order to avoid P, $In_{0.52}Al_{0.48}As$ lattice-matched to InP is produced in MBE as a substitute for InP.

InGaAsP/InP can be produced by LPE over the entire range of compositions without difficulty. This is because the amounts of Ga, As and P required in the In solution are easy to control (not too large distribution coefficients), as is shown in Fig. 32. On the other hand, large P/As flux ratios are necessary in MOVPE complicating the compositional control of InGaAsP, especially when the As content is small, i.e. $\lambda < 1.2\,\mu m$. Quaternary layers with $\lambda \approx 1.1\,\mu m$ are, however, of growing interest for waveguides.

7) The deposition efficiency η is the weight ratio of grown material to consumed source material. While in LPE growth takes place only on the epitaxial substrate, in MBE deposition takes place on the entire exposed surface and in MOVPE on the entire heated surface. For this and other reasons η is rather high in LPE, where it can even approach 100% if binary layers are grown from repeatedly used two-phase solutions. For the other epitaxial techniques η is very low. For instance, in a Varian Gen II MBE system 0.6 g of As are consumed per μm of grown GaAs using an As/Ga flux ratio of ≈ 20 [122]. This corresponds to $\eta = 1.0\%$ on a 2 inch wafer. For MOVPE the deposition efficiency is of the same order of magnitude or even less. Due to this LPE is the method of choice if thick layers ($> 2\,\mu m$) are to be grown.

8) The costs of an epitaxial growth system are low for LPE, but about 5 times as high for MOVPE and MBE.

9) Very little safety equipment is necessary for LPE and MBE. In LPE the hazard of a hydrogen explosion is limited to the small volume of the reactor tube provided that the H_2 bottles are stored outside the laboratory. Only a negligible quantity of toxic gases evaporates from the metallic solutions. The MBE process takes place in a closed vacuum chamber and, therefore, danger exists only when this is opened. MOVPE, however, is very hazardous. The hydrides PH_3 and AsH_3 commonly used are extremely toxic, and they are stored in cylinders under high pressure. Moreover, the metalorganic compounds are self-igniting in air. Therefore, in addition to the costs of the growth apparatus, expensive equip-

ment including high-capacity exhausts is necessary for MOVPE.

10) The epitaxial methods differ considerably with respect to environmental pollution. Due to its high deposition efficiency the LPE process is inherently less harmful to the environment than the other techniques. The waste metallic source material of LPE is solid, compact and unproblematic to dispose of since it is insoluble in water. Furthermore, the solvent material can be recycled. In MOVPE the high flux of toxic waste gases has either to be adsorbed in an activated carbon filter or washed in a scrubber by liquid chemicals or burned off. In either case end products remain whose final disposal is problematic because they are harmful to the environment.

11) LPE is well suited as an instrustrial process, especially for the production of green GaP LEDs, red AlGaAs LEDs and GaAs IREDs because of costs and device performance. Thick (70 μm) layers can be grown for this purpose by the dipping technique on one hundred 2 inch wafers in one LPE boat at the same time; see Sect. 2.1. The pn-junction in these single layers is formed by the temperature-dependent amphoteric incorporation of Si. The production costs of these layers including source materials and investment for the growth system are extremely low and amount only to 25% of the costs for the substrates. The hydride VPE process is also used for this purpose being only slightly more expensive than the LPE process, but the MOVPE and MBE processes are clearly ruled out on cost grounds. The brightness of these LPE devices is at least one order of magnitude higher than of those made by competing methods. The commonly accepted explanation for this difference is as follows: In the group-III-rich growth environment of LPE only few Ga vacancies are created. In the group-V-rich growth environment of all other epitaxial methods many Ga vacancies are created and, hence, complexes of As (or P) on Ga sites coupled to two Ga vacancies are formed, which act as luminescence killers.

5.2 Weaknesses of LPE

12) At present LPE appears not to be suited for the production of device structures involving very thin layers, superlattices or quantum wells, for instance MODFET structures. This is essentially due to the only moderate thickness control of thin layers. While GaAlAs DH lasers are now produced mainly by MOVPE and MBE and only to a lesser extent by LPE, InGaAsP lasers are still produced mainly by LPE because of the difficulties still existing with the other epitaxial techniques in this material system. The trend, however, goes in direction of MOVPE and gas source MBE. It is argued that in laser production the LPE process itself is indeed an inexpensive step, but the main costs arise from the testing procedure necessary on each individual device because of the variations in layer thickness.

13) A miscibility gap occurs in certain alloy systems when produced by LPE but not by the other epitaxial methods. This is again a consequence of LPE being an equilibrium process. This inhibits the growth of cer-

tain alloy compositions; for instance, $In_xGa_{1-x}As_ySb_{1-y}$ on GaSb or on InAs with $x \approx y \approx 0.5$ [109]. In the InGaAsP/InP and InGaAsP/GaAs systems, however, all lattice-matched compositions can be grown without phase separation owing to the stabilizing force of the substrate strain discussed in Sect. 4.3.

14) Strained-layer epitaxy is a promising area of investigation in MOVPE and MBE, but in LPE little success is expected since no coherent layers can be deposited if the relative lattice mismatch exceeds a few tenths of a percent.

15) The sharpness of GaAs/GaAlAs heterotransitions is about one monolayer (ML) for MBE and 1–3 ML for MOVPE. For LPE the interface sharpness as observed by high resolution TEM is ≈ 4 ML for InGaAsP grown on InP and ≈ 18 ML for InP grown on InGaAsP ($\lambda = 1.3 \mu m$) at $635° C$ [130]. The relatively large unevenness of the latter interface is attributed to the irregular back-dissolution of InGaAsP in the liquid during the initial stage of the InP growth.

16) This back-dissolution occurs because of the high solubility of As and Ga in the In solution, whereas in the former case almost no back-dissolution happens because of the low solubility of P in the growth solution. The back-dissolution increases with increasing content of As and Ga in the quaternary layer, and $\lambda = 1.5 \mu m$ lasers on (100)-oriented substrate can generally not be grown by LPE without an additional anti-meltback layer between the active and InP cladding layer. The danger of back-dissolution is even greater for growth on nonplanar surfaces, for instance growth of InP on InGaAsP gratings for DFB lasers. The back-dissolution can, however, be overcome by using Sn instead of In as a solvent as discussed in Sect. 4.1. This way InGaAs ($\lambda = 1.66 \mu m$) and InGaAsP ($\lambda = 1.53 \mu m$) lasers have been grown without an anti-meltback layer [86], and gratings in InGaAsP have been overgrown by InP nearly dissolution-free [87]. For the GaAs/AlGaAs system the problem of back-dissolution is less serious since the solubility of Al in Ga–As solutions is very low.

17) Growth of thin layers (< 100 nm) is easily achieved in MBE and MOVPE owing to the very low growth rate (0.1–3 nm/s) in these processes. In LPE, unfortunately, the growth rate is not constant in time and is the highest at the onset of growth; see Fig. 4. The thickness is 1.5–500 nm after the first second of growth; see (53). Therefore, control of thin layers is very difficult. The growth rate can be decreased by lowering the supersaturation, but then the tendency of back-dissolution is increased. As a consequence, a trade-off exists between minimal layer thickness and interface sharpness.

18) In atomic layer epitaxy (ALE) the growth of each monolayer is controlled by periodically interrupting the group III and group V fluxes. This technique is possible with MOVPE and MBE but not with LPE.

19) In the LPE process the control of layer thickness, especially for thin layers, is only moderate due to the effects discussed in Sects. 2.3 and 3.3. Therefore, LPE is considered to be applicable only for the production of single devices but not for integrated circuits. In MOVPE

and MBE, however, thickness variations of only 2% over a 2 inch wafer can be achieved [124].

20) The surface flatness of LPE layers strongly depends on the misorientation, supersaturation and dopant used. Although atomically flat epilayers can be obtained if the substrates are exactly oriented (Sect. 3.1), in general a terraced surface results due to step bunching. The steps, whose height is typically 20 nm, corresponding to a tenth of the active layer thickness in lasers, affect the far-field pattern of these devices. In addition, growth defects often result from unsolved particles floating on the solution, from graphite abrasion or from incomplete wipe-off of the solution.

Semi-insulating InP:Fe cannot be produced by LPE at a reasonable temperature [94] but is successfully grown by MOVPE.

In contrast to MBE, an in situ characterization of the growing layer is impossible in LPE, because the epilayer surface is hidden by the metallic solution. Also, other features of MBE like the production of intentionally graded layers, δ-doped layers or the combination of several processing steps in a common vacuum system cannot be performed by LPE.

6. Future Directions of LPE

Today more than 50% of the compound semiconductor devices produced are based on LPE material. However, we have to distinguish between simple and complicated devices. Simple devices are those utilizing not more than 2 or 3 epitaxial layers of several microns in thickness. These are essentially LEDs and IREDs based on GaAs and GaP, solar cells based on GaAs, and IR detectors based on CdHgTe and InGaAs/InP. Complicated devices are those where several very thin layers are required. Among these are all kinds of transistors, lasers and modern quantum-well devices.

For the simple devices LPE will retain its leading position in the future because of costs. One million chips are made from the layers grown every day in a single modern dipping boat system! Modern AlGaAs DH-LEDs emitting at 650 nm have external efficiencies of 5–20% compared to 0.4% for conventional GaAsP/GaAs LEDs made be VPE emitting at the same wavelength. AlGaAs cannot be made by VPE, and by MOVPE it is too expensive. A rapid expansion of the market for LEDs and IREDs can be expected because of their applications in opto-couplers, local area networks, display walls, telecommanders and automobile electronics. A simple estimate shows that automobile rear lights could well be made by LEDs: The usual electric bulbs of rear lights have a power of 10 W. Taking a light efficiency of the bulb of 5% and of the red filter of 20% yields 100 mW of red light which can also be produced by LEDs.

Among the II–VI compounds only CdHgTe is of industrial importance. It is used for photodiodes in IR cameras in the wavelength range 3–12 μm. Today the production of CdHgTe is mainly by LPE, where single layers are grown in dipping boat systems on CdZnTe substrates. The pn-junction is made by Hg diffusion or
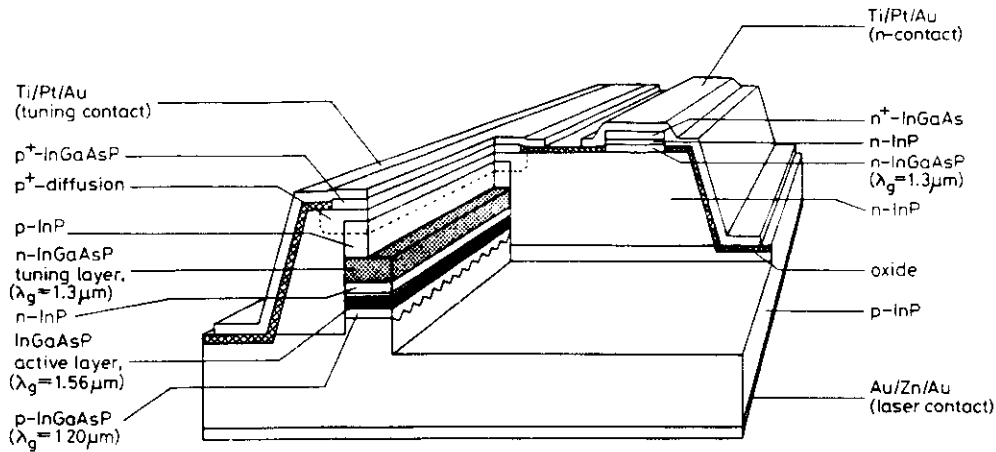
Fig. 38. Schematic structure of the $\lambda = 1.56\,\mu m$ InGaAsP/InP tunable twin-guide DFB laser after Schanen et al. [131]

by implantation. The trend is towards CdHgTe growth on the more reliable Si or GaAs substrates using buffer layers to accommodate the mismatch. This is being tried by MOVPE, LPE and hybrid epitaxy.

Concerning complicated GaAs-based devices it has to be stated that most of the GaAs lasers for compact disc players are made by LPE (especially in Japan), but that a trend exists towards the use of MBE and MOVPE. New devices like surface emitting lasers, GRINSCH lasers, MODFETs or ICs can be made exclusively by the latter techniques.

For complicated InP-based devices the situation is more favourable for LPE: Most quaternary lasers for optical telecommunication are still made by LPE. Figure 38 illustrates that even novel sophisticated devices like a tunable twin-guide laser grown by a three-step epitaxial process is made by LPE [131]. In this material system the breakthrough for MOVPE was only very recently, MBE cannot produce P-containing compounds, and GSMBE is still a few years behind. The trend towards MOVPE and GSMBE could, however, be reversed, e.g. if the production of the highly toxic arsine were forbidden, or if the deposition of toxic waste products were no longer possible due to stricter regulations. In such a case the harmless LPE process would be the only viable alternative.

Nearly all of the existing LPE growth systems are home-made and are not professional systems. Therefore, LPE has still a high potential for further development. If in future LPE systems can also be bought from specialized manufacturers, as is the case with MBE and MOVPE systems, we can expect radical improvements in terms of temperature control, substrate loading systems and large area growth. Then we can also hope to overcome the existing difficulties in reproducibly growing thin layers.

References

1. H. Nelson: Epitaxial growth from the liquid state and its application to the fabrication of tunnel and laser diodes. RCA Rev. 24, 603 (1963)
2. M.B. Panish, I. Hayashi, S. Sumski: Double-heterostructure injection lasers with room-temperature thresholds as low as 2300 A/cm². Appl. Phys. Lett. 16, 326 (1970)

3. Zh.I. Alferov, V.M. Andreev, D.Z. Garbuzov, Yu.V. Zhilyaev, E.P. Morozov, E.L. Portnoi, V.G. Trofim: Investigation of the influence of the AlAs–GaAs heterostructure parameters on the laser threshold current and the realization of continuous emission at room temperature. Sov. Phys. Semicond. 4, 1573 (1971)
4. J.J. Hsieh, J.A. Rossi, J.P. Donelly: Room-temperature cw operation of GaInAsP/InP double-heterostructure diode lasers emitting at 1.1 μm. Appl. Phys. Lett. 28, 709 (1976)
5. R.E. Nahory, M.A. Pollack, E.D. Beebe, J.C. DeWinter, R.W. Dixon: Continuous operation of 1.0-μm-wavelength GaAsSb/AlGaAsSb double-heterostructure injection lasers at room temperature. Appl. Phys. Lett. 28, 19 (1976)
6. L.M. Dolginov, L.V. Druzhinina, P.G. Eliseev, M.G. Milvidskii, B.N. Sverdlov: New uncooled injection heterolaser emitting in the 1.5–1.8 μm range. Sov. J. Quantum. Electron. 6, 257 (1976)
7. H.H. Wieder, A.R. Clawson, G.E. McWilliams: InGaAsP/InP heterojunction photodiodes. Appl. Phys. Lett. 31, 468 (1977)
8. R.F. Leheny, R.E. Nahory, M.A. Pollack: InGaAs pin photodiodes for long-wavelength fiber-optic systems. Electron. Lett. 15, 713 (1979)
9. T. Sukegawa, T. Hiraguchi, A. Tanaka, M. Hagino: Highly efficient p-GaSb/n-GaAlSb photodiodes. Appl. Phys. Lett. 32, 376 (1978)
10. C.E. Hurwitz, J.J. Hsieh: GaInAsP/InP avalanche photodiodes. Appl. Phys. Lett. 32, 487 (1978)
11. T.P. Pearsall, M. Papuchon: The GaInAs homojunction photodiode – A new avalanche photodetector in the near infrared between 1.0 and 1.6 μm. Appl. Phys. Lett. 33, 640 (1978)
12. H.D. Law, L.R. Tomasetta, K. Nakano, J.S. Harris: 1.0–1.4 μm high-speed avalanche photodiodes. Appl. Phys. Lett. 33, 416 (1978)
13. T. Kagawa, G. Motosugi: AlGaAsSb avalanche photodiodes for 1.0–1.3 μm wavelength region. Jpn. J. Appl. Phys. 18, 2317 (1979)
14. K. Mause, H. Salow, A. Schlachetzki, K.H. Bachem, K. Heime: Circuit integration with gate-controlled Gunn devices, in Proc. Int. Symp. Gallium Arsenide and related compounds, Boulder, Colorado. The Institute of Physics, London and Bristol, Conf. Ser. No. 17 (1972) p. 275
15. J. Katz, N. Bar-Chaim, P.C. Chen, S. Margalit, I Ury, D. Wilt, M. Yust, A. Yariv: A monolithic integration of GaAs/GaAlAs bipolar transistor and heterostructure laser. Appl. Phys. Lett. 37, 211 (1980)
16. R.F. Leheny, R.E. Nahory, M.A. Pollack, A.A. Ballman, E.D. Beebe, J.C. Dewinter, R.J. Martin: Integrated InGaAs pin FET photoreceiver. Electron. Lett. 16, 353 (1980)
17. D. Fritzsche, E. Kuphal, R. Aulbach: Fast response InP/InGaAsP heterojunction phototransistors. Electron. Lett. 17, 178 (1981)

18. H. Kawanishi, Y. Suematsu, K. Utaka, Y. Itaya, S. Arai: GaInAsP/InP injection laser partially loaded with first-order distributed Bragg reflector. IEEE J. QE-15, 701 (1979)

19. O. Mikami: 1.55 µm GaInAsP/InP distributed feedback lasers. Jpn. J. Appl. Phys. 20, L488 (1981)

20. H. Burkhard, E. Kuphal, H.W. Dinges: Extremely low threshold current 1.52 µm InGaAsP/InP MS-DFB lasers with second-order grating. Electron. Lett. 22, 802 (1986)

21. E.A. Rezek, R. Chin, N. Holonyak, Jr., S.W. Kirchoefer, R.M. Kolbas: Quantum-well InP-InGaPAs heterostructure lasers grown by liquid phase epitaxy. J. Electron. Mater. 9, 1 (1980)

22. W.T. Tsang, R.A. Logan: Observation of enhanced single longitudinal mode operation in 1.5-µm GaInAsP erbium-doped semiconductor injection lasers. Appl. Phys. Lett. 49, 1686 (1986)

23. L.R. Dawson: Liquid phase epitaxy, in Progr. in Solid-State Chemistry Vol. 7, ed. by H. Reiss, J.O. McCaldin (Pergamon, Oxford 1972) p. 117

24. M.B. Panish, M. Ilegems: Phase equilibria in ternary III–V systems, in Progr. in Solid-State Chemistry, Vol. 7, ed. by H. Reiss, J.O. McCaldin (Pergamon, Oxford 1972) p. 39

25. H. Kressel, H. Nelson: Properties and applications of III–V compound films deposited by liquid-phase epitaxy, in Physics of Thin Films, Vol. 7, ed. by. G. Hass, M.H. Francombe, R.W. Hoffman (Academic, New York 1973) p. 115

26. G.M. Blom, S.L. Blank, J.M. Woodall (eds.): Liquid Phase Epitaxy. Special issue of J. Crystal Growth, Vol. 27 (1974)

26a. E.A. Giess, R. Ghez: Liquid Phase Epitaxy, in Epitaxial Growth, Part A, ed. by J.W. Matthews (Academic, New York 1975) p. 183

27. H.C. Casey, Jr., M.B. Panish: Heterostructure Lasers, Part B (Academic, New York 1978) Chap. 6

28. K.W. Benz, E. Bauser: Growth of binary III–V semiconductors from metallic solutions, in: Crystals, Vol. 3 (Springer, Berlin, Heidelberg 1980) p. 1

29. J.J. Hsieh: Liquid-Phase Epitaxy, in Handbook of Semiconductors, Vol. 3, ed. by T.S. Moss (North-Holland, Amsterdam 1980) Chap. 6

30. G.B. Stringfellow: Epitaxy. Rep. Prog. Phys. 45, 469 (1982)

31. K. Nakajima: The liquid-phase epitaxial growth of InGaAsP, in: Semiconductors and Semimetals, Vol. 22, Part A, ed. by W.T. Tsang (Academic, New York 1985) p. 1

32. M.B. Small, R. Ghez: Growth and dissolution kinetics of III V heterostructures formed by LPE. J. Appl. Phys. 50, 5322 (1979); J. Appl. Phys. 51, 1589 (1980); J. Appl. Phys. 53, 4907 (1982); J. Appl. Phys. 55, 926 (1984)

33. G. Traeger, E. Kuphal, K.-H. Zschauer: Diffusion limited LPE growth of mixed crystals: Application to InGaAs on InP. J. Cryst. Growth 88, 205 (1988)

34. H.S. Carslaw, J.C. Jaeger: Conduction of Heat in Solids (Oxford University Press, London 1959)

35. J.J. Hsieh: Thickness and surface morphology of GaAs LPE layers grown by supercooling, step-cooling, equilibrium-cooling and two-phase solution techniques. J. Cryst. Growth 27, 49 (1974)

36. R.L. Moon: The influence of growth solution thickness on the LPE layer thickness and constitutional supercooling requirement for diffusion-limited growth. J. Cryst. Growth 27, 62 (1974)

37. B. De Cremoux: First-order theory of diffusion-limited growth in LPE: application to InGaAsP. Proc. Int. Symp. Gallium Arsenide and Related Compounds, Conf. Ser. No. 45 (Institute of Physics, Bristol 1979) p. 52

38. D. Pawlik: Thickness of GaAs and GaAlAs-LPE layers grown by linear cooling. Siemens Forsch. Entwickl. Ber. 7, 219 (1978)

39. D. Dutartre: LPE growth rate in AlGaAs system; theoretical and experimental analysis. J. Cryst. Growth 64, 268 (1983)

40. A. Doi, T. Asano, M. Migitaka: Epitaxial growth of GaAs from thin Ga solution. J. Appl. Phys. 47, 1589 (1976)

41. M.B. Panish: Phase equilibria in the system Al–Ga–As Sn and electrical properties of Sn-doped liquid phase epitaxial AlGaAs. J. Appl. Phys. 44, 2667 (1973)

42. G.B. Stringfellow: Calculation of ternary and quaternary III–V phase diagrams. J. Cryst. Growth 27, 21 (1974)

43. E. Kuphal, H.W. Dinges: Composition and refractive index of GaAlAs determined by ellipsometry. J. Appl. Phys. 50, 4196 (1979)

44. Landolt-Börnstein, New Series III/17a, ed. by O. Madelung (Springer, Berlin, Heidelberg 1982)

45. E. Kuphal: Phase diagrams of InGaAsP, InGaAs and InP lattice-matched to (100)InP. J. Cryst. Growth 67, 441 (1984)

46. M. Ilegems, M.B. Panish: Phase equilibria in III–V quaternary systems – Application to Al–Ga–P–As. J. Phys. Chem. Solids 35, 409 (1974)

47. A.S. Jordan, M. Ilegems: Solid-liquid equilibria for quaternary solid solution involving compound semiconductors in the regular solution approximation. J. Phys. Chem. Solids 36, 329 (1975)

48. B. De Cremoux: The crystallization path: A way to the GaInAsP phase diagram. IEEE J. QE-17, 123 (1981)

49. E. Perea, C. Fonstad: Phase diagram calculations for InGaPAs lattice matched to (111–B) InP in the temperature range 600–660° C. J. Appl. Phys. 51, 331 (1980)

50. J.J. Hsieh: Phase diagram for LPE growth of GaInAsP layers lattice matched to InP substrates. IEEE J. QE-17, 118 (1981)

51. J.J. Hsieh: Thickness of InP layers grown by LPE from supercooled solutions. Proc. Int. Symp. on Gallium Arsenide and Related Compounds, St. Louis, The Institute of Physics, London and Bristol, Inst. Phys. Conf. Ser. 33b, 74, 1977

52. R.E. Nahory, M.A. Pollack, W.D. Johnston, Jr.: Band gap versus composition and demonstration of Vegard's law for InGaAsP lattice matched to InP. Appl. Phys. Lett 33, 659 (1978)

53. N. Pan, N. Tabatabaie, G.E. Stillman: LPE diffusion-limited growth of InGaAs. J. Cryst. Growth 78, 97 (1986)

54. E. Kuphal: To be published

55. E. Grobe, H. Salow: Der Aufbau epitaktischer GaAs-Schichten aus der flüssigen Phase. Z. angew. Phys. 32, 381 (1972)

56. E. Bauser, M. Frik, K.S. Loechner, L. Schmidt, R. Ulrich: Substrate orientation and surface morphology of GaAs liquid phase epitaxial layers. J. Cryst. Growth 27, 148 (1974)

57. E. Kuphal: The influence of graphite boat material on the purity of LPE InGaAs. Appl. Phys. A 43, 37 (1987)

58. L.M.F. Kaufmann, K. Heime: A new graphite boat construction for the LPE growth of thin GaAs layers with a new technique. J. Cryst. Growth 42, 321 (1977)

59. L.M.F. Kaufmann, R. Tilders, K. Heime: University of Duisburg, private communication

60. D.E. Holmes, G.S. Kamath: Growth of InP by infinite solution LPE. J. Cryst. Growth 54, 51 (1981)

61. H.J. Scheel: A new technique for multilayer LPE. J. Cryst. Growth 42, 301 (1977)

62. H.J. Scheel: Atomically flat surfaces and p-n junctions of GaAs by LPE, E-MRS Meeting, XVI, 175, Les Editions des Physique, Paris, 1987

63. Zh.I. Alferov, V.M. Andreev, V.I. Korol'kov, E.L. Portnoi, D.N. Tret'yakov: Coherent radiation of epitaxial heterojunction structures in the AlAs-GaAs system. Soviet Phys.-Semicond. 2, 1289 (1969)

64. H. Burkhard, E. Kuphal, H.W. Dinges: Erzeugung und Untersuchung von Halbleiterlasern aus dem System InGaAsP/InP für die optische Nachrichtentechnik, Mitteilungen aus dem Forschungsinstitut der Deutschen Bundespost (Heft 12) 1988

65. G.A. Antypas: Prevention of InP surface decomposition in liquid phase epitaxial growth. Appl. Phys. Lett. 37, 64 (1980)

66. E. Kuphal: Phase diagram and LPE of the system In-P-Sn, E-MRS Meeting, XVI, 201, Les Editions de Physique, Paris, 1987

67. B.H. Chin, G.P. Schwartz, W.C. Dautremont-Smith, J.R. Dick: Preservation of Indium Phosphide substrates. J. Electrochem. Soc. 133, 2161 (1986)

68. K. Pfanner, D. Franke, B. Sartorius, M. Schlak: A comparative study on protection methods against InP substrate decomposition in liquid phase epitaxy. J. Cryst. Growth 88, 67 (1988)

69. E. Kuphal, A. Altenrath: Wachstum von Eisen-dotierten semi-isolierenden InGaAs-Schichten mittels Flüssigphasenepitaxie. Techn. Rep. 65 TBr 27. Deutsche Bundespost, 1988

70. E. Kuphal: Unpublished result

71. M.G. Astles, H. Hill, V.W. Steward: An experimental investigation of edge-growth effects in the LPE growth of GaAs and GaAlAs. J. Cryst. Growth 62, 61 (1983)

72. M.C. Tamargo, C.L. Reynolds, Jr., R.I. Kunkel: Thermal effects on LPE layer thickness. J. Cryst. Growth 71, 421 (1985)

73. R.B. Wilson, P. Besomi, R.J. Nelson: Investigation of melt carry-over during liquid phase epitaxy. J. Electrochem. Soc. 132, 172 (1985)

74. U. König, W. Keck: Contact angles between III–V melts and several substrates. J. Electrochem. Soc. 130, 685 (1983)

75. Zh.I. Alferov, D.Z. Garbuzov, I.N. Arsent'ev, B.Ya. Ber, L.S. Vavilova, V.V. Krasovskii, A.V. Chudinov: Auger profiles of the composition and luminescence studies of liquid-phase grown InGaAsP heterostructures with $(1.5-5) \times 10^{-6}$ cm active regions. Sov. Phys. Semicond. 19, 679 (1985)

76. J. Heinen: Simultaneous liquid phase epitaxial growth of multilayer structures in a multislice boat. J. Cryst. Growth 58, 596 (1982)

77. B.V. Dutt, D.D. Roccasecca, H. Temkin, W.A. Bonner: A novel multi-slice LPE boat. J. Cryst. Growth 66, 525 (1984)

78. J.M. Woodall: Solution grown $Ga_{1-x}Al_xAs$ superlattice structures. J. Cryst. Growth 12, 32 (1972)

79. G.H.B. Thompson, P.A. Kirkby: Liquid phase epitaxial growth of six-layer GaAs/(GaAl)As structures for injection lasers with 0.04 μm thick centre layer. J. Cryst. Growth 27, 70 (1974)

80. E. Bauser, L. Schmidt, K.S. Löchner, E. Raabe: Liquid phase epitaxy apparatus for multiple layers utilizing centrifugal forces, Jpn. J. Appl. Phys. 16, Suppl. 16-1, 457 (1977)

81. A.W. Nelson, E.A.D. White: Improvements to melt preparation in LPE growth of semiconductor heterostructures. J. Cryst. Growth 57, 610 (1982)

82. E. Bauser, H.P. Strunk: Microscopic growth mechanisms of semiconductors: experiments and models. J. Cryst. Growth 69, 561 (1984)

83. U. Morlock, M. Kelsch, E. Bauser: Extremely flat layer surfaces in liquid phase epitaxy of GaAs and AlGaAs. J. Cryst. Growth 87, 343 (1988)

84. N. Chand, A.V. Syrbu, P.A. Houston: LPE growth effects of InP, InGaAs and InGaAsP on structured InP substrates. J. Cryst. Growth 61, 53 (1983)

85. S.H. Groves, M.C. Plonko: n^+-InP growth on InGaAs by liquid phase epitaxy. Appl. Phys. Lett. 38, 1003 (1981)

86. H. Burkhard, E. Kuphal: Three- and four-layer LPE InGaAs(P) mushroom stripe lasers for $\lambda = 1.30$, 1.54, and 1,66 μm. IEEE J. QE-21, 650 (1985)

87. E. Kuphal: Nearly back-dissolution-free LPE growth from Sn solutions over gratings for DFB lasers. Electron. Lett. 25, 1581 (1989)

88. E. Kuphal, D. Fritzsche: LPE growth of high purity InP and n- and p-$In_{0.53}Ga_{0.47}As$. J. Electron. Mater. 12, 743 (1983)

89. W. Walukiewicz, J. Lagowski, L. Jastrzebski, P. Rava, M. Lichtensteiger, C.H. Gatos, H.C. Gatos: Electron mobility and free-carrier absorption in InP; determination of the compensation ratio. J. Appl. Phys. 51, 2659 (1980)

90. M.S. Skolnick, P.J. Dean, S.H. Groves, E. Kuphal: Donor identification in liquid phase epitaxial indium phosphide. Appl. Phys. Lett 45, 962 (1984)

91. E. Kuphal: Preparation and characterization of LPE InP. J. Cryst. Growth 54, 117 (1981)

92. H. Nickel, E. Kuphal: Deep level spectroscopy and Schottky barrier characteristics of LPE n- and p-InP. Phys. Status Solidi (a) 65, 583 (1981)

93. M.G. Astles, F.G.H. Smith, E.W. Williams: Indium phosphide. II. Liquid epitaxial growth. J. Electrochem. Soc. 120, 1750 (1973)

94. M. Sugawara, M. Kondo, K. Nakai, A. Yamaguchi, K. Nakajima: Activation ratio of Fe in Fe-doped semi-insulating InP epitaxial layers grown by liquid phase epitaxy and metalorganic chemical vapor deposition. Appl. Phys. Lett. 50, 1432 (1987)

95. Y. Takeda, A. Sasaki: Composition latching phenomenon and lattice mismatch effects in LPE-grown $In_{1-x}Ga_xAs$ on InP substrate. J. Cryst. Growth 45, 257 (1978)

96. G.B. Stringfellow: The importance of lattice mismatch in the growth of $Ga_xIn_{1-x}P$ epitaxial crystals. J. Appl. Phys. 43, 3455 (1972)

97. M.C. Joncour, J.L. Benchimol, J. Burgeat, M. Quillec: Liquid phase epitaxial growth of $In_xGa_{1-x}As/InP$ near solid instability. J. de Phys. 43, Coll. C5-3 (1982)

98. J.D. Oliver, L.F. Eastman: Liquid phase epitaxial growth and characterization of high purity lattice matched $Ga_xIn_{1-x}As$ on (111)B InP. J. Electron. Mater. 9, 693 (1980)

99. T. Amano, K. Takahei, H. Nagai: Effect of baking temperature on purity of LPE $Ga_{0.47}In_{0.53}As$. Jpn. J. Appl. Phys. 20, 2105 (1981)

100. L.W. Cook, M.M. Tashima, N. Tabatabaie, T.S. Low, G.E. Stillman: High purity InP and InGaAsP grown by liquid phase epitaxy. J. Cryst. Growth 56, 475 (1982)

101. K.-H. Goetz, D. Bimberg, H. Jürgensen, J. Selders, A.V. Solomonov, G.F. Glinskii, M. Razeghi: Optical and crystallographic properties and impurity incorporation of $Ga_xIn_{1-x}As$ $(0.44 < x < 0.49)$ grown by liquid phase epitaxy, vapor phase epitaxy, and metal organic chemical vapor deposition. J. Appl. Phys. 54, 4543 (1983)

102. J.L. Benchimol, M. Quillec, C. LeCornec, G. LeRoux: The In–Ga–As–Zn system: LPE growth conditions for lattice matching on (111)B InP substrates. Appl. Phys. Lett 36, 454 (1980)

103. T.P. Pearsall: $Ga_{0.47}In_{0.53}As$: A ternary semiconductor for photodetector applications. IEEE J. QE-16, 709 (1980)

104. Y. Takeda, M. Kuzuhara, A. Sasaki: Properties of Zn-doped p-type $In_{0.53}Ga_{0.47}As$ on InP substrate. Jpn. J. Appl. Phys. 19, 899 (1980)

105. M.M. Tashima, L.W. Cook, G.E. Stillman: Room-temperature electron diffusion lengths in liquid phase epitaxial InGaAsP and InGaAs. Appl. Phys. Lett 39, 960 (1981)

106. P.W. Yu, E. Kuphal: Photoluminescence of Mn-doped and undoped $Ga_{0.47}In_{0.53}As$ on InP. Solid State Commun. 49, 907 (1984)

107. N. Chand, P.A. Houston, P.N. Robson: Mn as a p-type dopant in $In_{0.53}Ga_{0.47}As$ on InP substrates. Electron. Lett. 17, 726 (1981)

108. F. Fiedler, H.H. Wehmann, A. Schlachetzki: Growth and doping of InGaAsP/InP by liquid-phase epitaxy. J. Cryst. Growth 74, 27 (1986)

109. K. Onabe: Unstable regions in III–V quaternary solid solutions composition plane calculated with strictly regular solution approximation. Jpn. J. Appl. Phys. 21, L323 (1982)

110. B. De Cremoux, P. Hirtz, J. Ricciardi: On the presence of a solid immiscibility domain in the GaInAsP phase diagram. The Institute of Physics, London and Bristol, Conf. Ser. No. 56 (1981) p. 115

111. K. Onabe: Calculation of miscibility gap in quaternary InGaAsP with strictly regular solution approximation. Jpn. J. Appl. Phys. 21, 797 (1982)

112. G.B. Stringfellow: Miscibility gaps in quaternary III/V alloys. J. Cryst. Growth 58, 194 (1982)

113. G.B. Stringfellow: Spinodal decomposition and clustering in III/V alloys. J. Electron. Mater. 11, 903 (1982)

114. K. Takahei, H. Nagai: Instability of In–Ga–As–P liquid solution during low temperature LPE of $In_{1-x}Ga_xAs_{1-y}P_y$ on InP. Jpn. J. Appl. Phys. 20, L313 (1981)

115. P. Henoc, A. Izrael, M. Quillec, H. Launois: Composition modulation in liquid phase epitaxial InGaAsP layers lattice matched to InP substrates. Appl. Phys. Lett 40, 963 (1982)

116. E. Kuphal, A. Pöcker: LPE growth of high purity InP and $In_{1-x}Ga_xP_{1-y}As_y$. J. Cryst. Growth 58, 133 (1982)

117. G. Schemmel, R. Dorn, K. Hess, R. Linnebach, K. Lösch: LPE growth and characteristics of GaInAsP/InP structures for

photodetectors. The Institute of Physics, London and Bristol, Conf. Ser. No. 65 (1983) p. 209

118. J.L. Benchimol, M. Quillec, S. Slempkes: Improved mobility in InGaAsP alloys using high temperature LPE. J. Cryst. Growth **64**, 96 (1983)

119. P.D. Greene, S.A. Wheeler, A.R. Adams, A.N. El-Sabbahy, C.N. Ahmad: Background carrier concentration and electron mobility in LPE $In_{1-x}Ga_xAs_yP_{1-y}$ layers. Appl. Phys. Lett **35**, 78 (1979)

120. R.F. Leheny, A.A. Ballman, J.C. DeWinter, R.E. Nahory, M.A. Pollack: Compositional dependence of the electron mobility in $In_{1-x}Ga_xAs_yP_{1-y}$. J. Electron. Mater. **9**, 561 (1980)

121. H. Kamei, G. Sasaki, T. Kato, H. Hayashi, K. Ono, K. Yoshida: Growth of $Ga_{1-x}In_xAs$ layers with excellent compositional uniformity on InP by OMVPE. Institute of Physics, Bristol, Conf. Ser. No. 83 (1986) p. 183

122. G. Weimann, FTZ Darmstadt: Unpublished result

123. C. Ferrari, P. Franzosi, L. Gastaldi, F. Taiariol: Crystal quality investigation of InGaAs/InP and InGaAlAs/InP single heterostructures grown by molecular-beam epitaxy. J. Appl. Phys. **63**, 2628 (1988)

124. H. Nickel, FTZ Darmstadt: Unpublished result

125. K. Mizuishi, M. Hirao, S. Tsuji, H. Sato, M. Nakamura: Accelerated aging characteristics of InGaAsP/InP buried het-

erostructure lasers emitting at 1.3 µm. Jpn. J. Appl. Phys. **19**, L429 (1980)

126. I. Mito, M. Kitamura, K. Kobayashi, S. Murata, M. Seki, Y. Odagiri, H. Nishimoto, M. Yamaguchi, K. Kobayashi: InGaAsP double-channel-planar-buried-heterostructure laser diode (DC-PBH LD) with effective current confinement. J. LT-1, 195 (1983)

127. H. Ishikawa, H. Imai, T. Tanahashi, K. Hori, K. Takahei: V-grooved substrate buried heterostructure InGaAsP/InP laser emitting at 1.3 µm wavelength. IEEE J. QE-**18**, 1704 (1982)

128. E. Oomura, H. Higuchi, Y. Sakakibara, R. Hirano, H. Namizaki, W. Susaki, K. Ikeda, K. Kujikawa: InGaAsP/InP buried crescent laser diode emitting at 1.3 µm wavelength. IEEE J. QE-**20**, 866 (1984)

129. Y.Z. Liu, C.C. Wang, M. Chu: Low threshold 1.3-µm InGaAsP/InP lasers prepared by a single-step liquid-phase epitaxy. J. Appl. Phys. **63**, 2151 (1988)

130. N. Kuwano, T. Goto, K. Oki, S. Uchiyama, K. Iga: Electron microscopic observation of heterointerface in $Ga_xIn_{1-x}As_yP_{1-y}$/InP grown by liquid phase epitaxy. Jpn. J. Appl. Phys. **27**, 1768 (1988)

131. C.F.J. Schanen, S. Illek, H. Lang, W. Thulke, M.C. Amann: Fabrication and lasing characteristics of $\lambda = 1.56$ µm tunable twin-guide (TTG) DFB lasers. IEE Proc. **137**. Pt. J. (1990) p. 69